



HAL
open science

Low-Pass NGD Numerical Function and STM32 MCU Emulation Test

Blaise Ravelo, Mathieu Guerin, Wenceslas Rahajandraibe, Valentin Gies, Lala Rajaoarisoa, Sebastien Lallechere

► **To cite this version:**

Blaise Ravelo, Mathieu Guerin, Wenceslas Rahajandraibe, Valentin Gies, Lala Rajaoarisoa, et al.. Low-Pass NGD Numerical Function and STM32 MCU Emulation Test. IEEE Transactions on Industrial Electronics, 2022, 69 (8), pp.8346 - 8355. 10.1109/TIE.2021.3109543 . hal-03509432

HAL Id: hal-03509432

<https://hal.science/hal-03509432v1>

Submitted on 7 Mar 2023

HAL is a multi-disciplinary open access archive for the deposit and dissemination of scientific research documents, whether they are published or not. The documents may come from teaching and research institutions in France or abroad, or from public or private research centers.

L'archive ouverte pluridisciplinaire **HAL**, est destinée au dépôt et à la diffusion de documents scientifiques de niveau recherche, publiés ou non, émanant des établissements d'enseignement et de recherche français ou étrangers, des laboratoires publics ou privés.





GENERAL INSTRUCTION

- **Authors: Carefully check the page proofs (and coordinate with all authors); additional changes or updates WILL NOT be accepted after the article is published online/print in its final form. Please check author names and affiliations, funding, as well as the overall article for any errors prior to sending in your author proof corrections.**
- **Authors: We cannot accept new source files as corrections for your article. If possible, please annotate the PDF proof we have sent you with your corrections and upload it via the Author Gateway. Alternatively, you may send us your corrections in list format. You may also upload revised graphics via the Author Gateway.**
- **Authors: Unless invited or otherwise informed, there is a mandatory Excessive Article Length charge of \$250 per page (\$200 for IES members) in excess of eight (8) pages. If you have any questions regarding overlength page charges, need an invoice, or have any other billing questions, please contact apcinquries@ieee.org as they handle these billing requests.**

QUERIES

- Q1. Author: Please provide the expansion for the acronym DAC.
- Q2. Author: Please provide the ORCID for the corresponding author Mathieu Guerin.
- Q3. Author: Please update the Ref. [37]
- Q4. Author: Please provide the educational details (degree/university/location/subject) for author Blaise Ravelo.
- Q5. Author: Please check whether the biography of author Mathieu Guerin is correct as set.
- Q6. Author: Please provide the subject in which the author Mathieu Guerin received the doctorate degree.
- Q7. Author: Please provide the year in which the author Wenceslas Rahajandraibe received the Ph.D. degree.

Low-Pass NGD Numerical Function and STM32 MCU Emulation Test

Blaise Ravelo , Member, IEEE, Mathieu Guerin, Member, IEEE,
 Wenceslas Rahajandraibe , Member, IEEE, Valentin Gies, Member, IEEE,
 Lala Rajaoarisoa , Member, IEEE, and Sébastien Lalléchère , Member, IEEE

Abstract—This article introduces an original microcontroller unit (MCU) design of numerical low-pass (LP) negative group delay (NGD) function. The innovative theory of the numerical LP-NGD function is developed based on the first-order analog transfer function discretization. The infinite impulse response (IIR) LP-NGD is fundamentally formulated in function of the desired NGD value, cutoff frequency, gain, and the MCU sampling frequency. A STM32 MCU proof-of-concept (POC) is tested to implement the IIR LP-NGD function. Different real-time tests with visualization of input and output analog signals from the MCU LP-NGD POC were performed. As expected, time-advance demonstration tests with milli-second short- and several hour long-duration time-scale with arbitrary waveform signals from temperature and humidity sensors. The signal time-advance is not in contradiction with the causality. The proposed digital MCU function opens a potential future industrial application of LP-NGD function via sensed signal anticipation.

Index Terms—Circuit design, emulation, microcontroller unit (MCU), negative group delay (NGD), numerical circuit, time-domain demonstration.

I. INTRODUCTION

IN EARLY age of Industry 4.0 revolution, the role of remote communication is one of the design research engineer breakthrough [1]. The delay effect plays a major role on the communication system general performance [2]–[4]. For example, these effects are critical for reliable operation of remote-control

Manuscript received March 29, 2021; revised June 17, 2021 and July 3, 2021; accepted August 23, 2021. (Corresponding author: Mathieu Guerin.)

Blaise Ravelo is with the Nanjing University of Information Science and Technology, Nanjing 210044, China (e-mail: blaise.ravelo@yahoo.fr).

Mathieu Guerin, Wenceslas Rahajandraibe, and Valentin Gies are with the CNRS, University of Toulon, 83130 Marseille, France, and also with the Aix-Marseille University, 3007 Marseille, France (e-mail: mathieu.guerin@im2np.fr; wenceslas.rahajandraibe@im2np.fr; valentin.gies@im2np.fr).

Lala Rajaoarisoa is with the IMT Lille Douai, Institut Mines-Télécom, Centre for Digital Systems, University Lille, F-59000 Lille, France (e-mail: lala.rajaoarisoa@imt-lille-douai.fr).

Sébastien Lalléchère is with the Institute Pascal, SIGMA Clermont, Université Clermont Auvergne, 63001 Clermont Ferrand, France (e-mail: sebastien.lallechere@uca.fr).

Color versions of one or more figures in this article are available at <https://doi.org/10.1109/TIE.2021.3109543>.

Digital Object Identifier 10.1109/TIE.2021.3109543

system. The quality of service (QoS) of remote sensing systems forecasted Industry 4.0 factories to operate correctly depends undeniably on the delay effects. The networked modern industrial sensing systems present an open risk of anomaly detection because of unintentional delays. So far, no rigorous solution is available to overcome the time delay effects in almost all areas of engineering [2]–[9].

One can cite different challenges to be overcome to face up the delay impacts. The signal delay degrades the digital communication QoS due to the wireless propagation channel dispersion and data desynchronization [3]–[4]. In the area of automation and control engineering, different industrial application examples as optimal vehicle activities [5], networked control system, and power system damping control [6] present performance limitations because of the delay effect. Time-domain analyses confirm that the stability of dynamic systems depend unavoidably to the feedback delays [7].

To take into account the delay effects on the system performance, analytical, and modeling methods for the enhancement of printed circuit board (PCB) signal integrity were proposed [8]–[11]. Delay estimation techniques were developed for estimating communication system performance [3]. Diverse estimation techniques based on complex analytical signals [12] have been developed. In addition to the noise effect issues, the group delay (GD) limits undesirably the communication performances [13]–[14].

In the area of biomedical engineering, under the telemedicine revolution, new generation of wearable biosensors is currently developed [15]. The delay effects play also a vital role on the performance of the wearable sensor signal monitoring. An innovative photoplethysmography signal measurements of respiration, oxygen, and blood pressure rate measurement were proposed [16]–[18]. A technique allowing to use an optimal number and positioning of multiple accelerometers for respiratory waveform estimation is developed in [19]. To improve the medical sensor performances, an advanced signal detection technique using negative GD (NGD) function is developed in [20]. Under the same challenge, an NGD predictor based on anticipatory relax dynamics using basically a delayed induced feedback function is proposed in [21] and [22].

In electronics engineering, NGD microwave monolithic integrated circuits have been employed to equalize the undesirable signal degradations as regularly found in the PCBs [23]. This NGD equalization technique was initiated in [24] for RC-effect

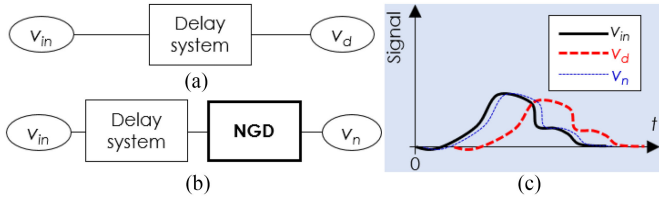


Fig. 1. Illustration scenario of NGD application. (a) Delay penalizing system. (b) NGD corrected system. (c) Input and output signal chronogram.

and to cancel out the signal delay. Fig. 1 illustrates a scenario of signal delay cancellation NGD application with delay system. Because of the NGD function, the delay between input signal v_{in} and output signal v_d is larger than that of v_{in} and v_n [$\text{delay}(v_{in}, v_d) \gg \text{delay}(v_{in}, v_n)$].

The technique was introduced in [25] to target industrial applications by overcoming multisensor time-delays. Acting as an unfamiliar function, it is worth to define what is the NGD function meaning. To answer to this curiosity, a brief state of the art about the NGD function will be described in the following paragraph.

The NGD phenomenon was initially validated with low-frequency (LF) electronic circuits in 1990s [26], [27]. Despite the counterintuitive aspect, the NGD circuits can be designed and implemented like classical and familiar electrical circuits as filters, amplifiers, phase shifters, oscillators. The LF NGD topologies proposed initially in [26]–[29] were built with classical electronic passive (R, L, and C) and operational amplifier components. The NGD phenomenon meaning was illustrated with time-domain experimentations showing the possibility to propagate the NGD output signal in time-advance with the input one [26]–[29]. This demonstration was realized with PCB showing an NGD output lamp lightened on before the input one [29]. This counterintuitive NGD phenomenon is not in contradiction with the causality principle [26]–[29]. For further understanding about the NGD concept, an investigation on the similitude between the NGD and linear filter gain behaviors is introduced in [30]. The concept of low-pass (LP) [31], [32] NGD function was initiated. Despite the research work progress in the area of electronics engineering, the NGD function remains an unmaturred concept for most of industrial engineers. Open questions are regularly asked about the industrial potential applications of the NGD function.

For this reason, a completely original research work on the design of numerical LP NGD circuit is developed in the present paper. The LP-NGD function is implemented on microcontroller unit (MCU) operating in different time scales. The NGD function can be potentially used as a pioneer work of anticipator for the real-time predetection of actuator and sensor faults and intelligent system diagnoses [33], [34]. The research work originality relies on the MCU numerical LP-NGD function design and test. For the better understanding, this paper is organized in three main sections. Section II will describe the numerical LP-NGD transfer function (TF) theory. Section III will present the LP-NGD MCU demonstrator as proof-of-concept (POC). Finally, Section IV concludes this article.

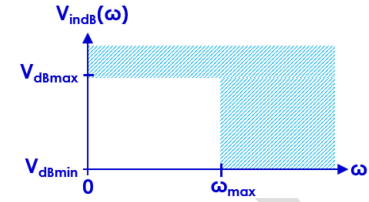


Fig. 2. Specific characterization diagram of numerical LP-NGD input signal.

II. MCU DESIGN PRINCIPLE OF DISCRETE LP NGD FUNCTION

Acting as one of the most unfamiliar digital function available in the literature, it would be necessary to define the operating input signal specifications before the theorization of the discrete LP-NGD TF.

A. Input Signal and MCU Specifications

A LP-NGD function is dedicated to operate with base band signal, which can be noticed by v_{in} . The ideal specifications of its frequency spectrum magnitude in dB of $V_{in}(j\omega)$ are illustrated in Fig. 2 by denoting the angular frequency variable ω . In this diagram, the signal spectrum magnitude is assumed $V_{in} = 0$ in the forbidden zone represented by the shadowed area. Signal v_{in} can present any arbitrary waveform but should be limited bandwidth denoted ω_{max} . The signal minimal and maximal strengths, denoted by V_{min} and V_{max} , need to be defined.

The MCU architecture is assumed powered by $V_{dd} = V_0$. It is mainly constituted by the block of computing core interfaced by analog digital converters (ADC) and DAC as input and output interfaces, respectively. The MCU operation is cadenced by its internal clock generating the sampling clock supposed with period denoted $T_s = 1/f_s$ (f_s is the sampling frequency). Given the case of input signal duration t_{max} , the MCU must operate with time step following the integer index $k = 0, 1, 2, \dots, k_{max} = \text{Ent}[t_{max}/T_s]$ by denoting $\text{Ent}[x]$ the superior integer part of real positive x . The discrete input and output signals at the instant time $t = kT_s$ are represented by

$$\begin{cases} v_{in}(k) = v_{in}(kT_s) \\ v_{out}(k) = v_{out}(kT_s) \end{cases} \quad (1)$$

B. Theoretical Investigation of Discrete LP-NGD Function

This section describes the main specifications and characterization of numerical LP-NGD function.

1) NGD Specifications: The NGD TF can be represented as a single-input single-output block diagram, as shown in Fig. 3(a). With the Laplace variable s , the associated analog TF can be formulated by $N(s) = V_{out}(s)/V_{in}(s)$. The NGD analysis in the frequency domain is based on the consideration of magnitude response, $N(\omega) = |N(j\omega)|$ and the GD defined by

$$\tau(\omega) = -\partial\varphi(\omega)/\partial\omega \quad (2)$$

with

$$\varphi(\omega) = \arctan \{ \text{Im} [N(j\omega)] / \text{Re} [N(j\omega)] \}. \quad (3)$$

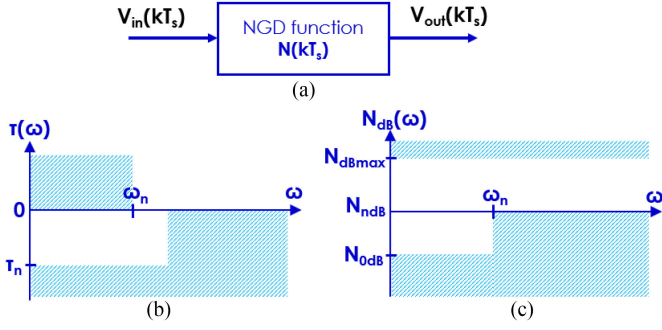


Fig. 3. (a) Block, (b) GD, and (c) magnitude response diagrams of LP-NGD function.

Fig. 3(b) represents the GD diagram specific to the ideal LP-NGD function, which is defined by two fundamental characteristics as follows.

- 1) The NGD value at very low frequencies

$$\tau_n = \tau(\omega \approx 0) < 0. \quad (4)$$

- 2) The NGD cutoff angular frequency $\omega_n = 2\pi f_n$, which is a root of the equation $\tau(\omega) = 0$.

Fig. 3(c) highlights the LP-NGD magnitude response specifications. For the case of first order linear NGD system (which will be explored in the following paragraph), it associates three main characteristics.

- 3) The minimal magnitude $N_{dBmin} = N_{0dB} = N_{dB}(\omega \approx 0)$, which should correspond to the magnitude at very LFs.
- 4) The maximal magnitude $N_{dBmax} = N_{dB}(\omega \approx \infty)$, which should be reached at very high frequencies.
- 5) And the magnitude $N_{ndB} = N_{dB}(\omega = \omega_n)$ at cutoff frequency.

2) Canonical Form of First Order LP-NGD TF: With the real parameters defined previously N_n , τ_n , and ω_n , the canonical form of LP-NGD analog TF is defined as [31]

$$N(s) = N_n(1 + \tau_a s)/(1 + \tau_b s) \quad (5)$$

where

$$\tau_a = \left(\sqrt{\tau_n^2 + 4/\omega_n^2} - \tau_n \right) / 2 \quad (6)$$

$$\tau_b = \left(\sqrt{\tau_n^2 + 4/\omega_n^2} + \tau_n \right) / 2. \quad (7)$$

The integrity between NGD input and output signals, v_{in} and v_{out} can be quantified with the quantity $M_n = N(\omega_n)$. The LP-NGD bandwidth magnitude flatness and maximal flatness factor can be assessed by the ratio, respectively, as follows:

$$\xi(\varpi) = M_n(\varpi)/N_n \quad (8)$$

$$\xi_{max}(\varpi) = N_{max}(\varpi)/N_n \quad (9)$$

where the NGD value-bandwidth product

$$\varpi = -\omega_n \tau_n. \quad (10)$$

By considering the LP-NGD TF expressed in (5), the previous magnitude flatness factors are rewritten as

$$\xi(\varpi)$$

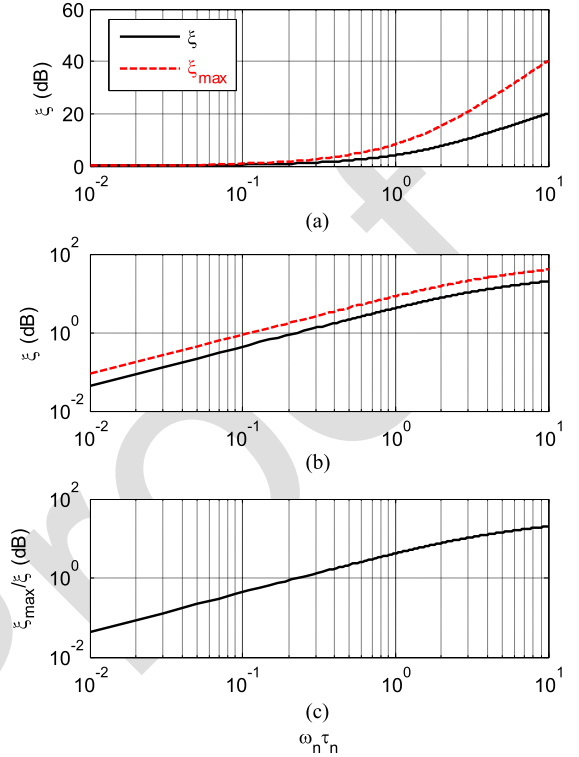


Fig. 4. LP-NGD TF magnitude flatness versus product $\omega_n \tau_n$ in (a) semilog x-axis, (b) log-log plots, and (c) ratio from (9).

$$= \left[\sqrt{4 + (\sqrt{\varpi^2 + 4} + \varpi)^2} \right] / \left[\sqrt{4 + (\sqrt{\varpi^2 + 4} - \varpi)^2} \right] \quad (11)$$

$$\xi_{max}(\varpi) = (\sqrt{\varpi^2 + 4} + \varpi) / (\sqrt{\varpi^2 + 4} - \varpi). \quad (12)$$

3) Characterization of LP-NGD TF Flatness: The magnitude flatness constitutes one of the main parameters affecting the LP-NGD function performance. It is particularly important to investigate the LP-NGD TF magnitude variation range in the NGD frequency band. Following this point, we considered the general plot of the flatness defined by (11). Fig. 4 displays the plots of these magnitude fastness factors in function of the NGD value-bandwidth product varied from 0.01 to 10. The flatness differences varied from 0 to 19 dB and we have $N_{max}/N_n > 1$ because $\tau_n < 0$.

C. LP-NGD Numerical Function Expression

The original numerical LP-NGD function is originally elaborated from the first-order LP-NGD canonical TF given in (5). Indeed, the TF equivalent discrete form is derived from the equivalent differential equation governing input v_{in} and output v_{out} . To realize the time-advance behavior related to the LP-NGD function, the input signal bandwidth should respect condition $\omega_{max} \leq \omega_n$. The analytical combination of $N(s)$ definition and TF (5) implies the Laplace symbolic equation

$$V_{out}(s) - N_n V_{in}(s) = s [N_n \tau_a V_{in}(s) - \tau_b V_{out}(s)]. \quad (13)$$

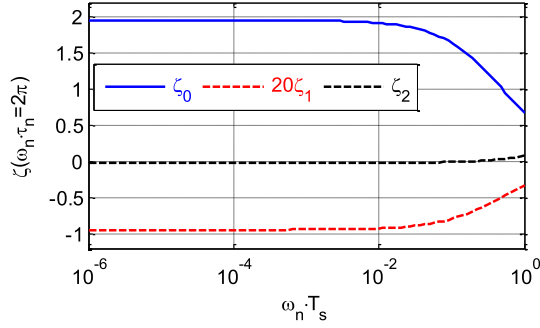


Fig. 5. Variations of LP-NGD IIR coefficients versus product $\omega_n T_s$.

By supposing that the input signal is generated under the initial condition $v_{in}(t = 0) = 0$. It can be derived with Laplace inverse transform the time-dependent differential equation

$$v_{out}(t) - N_n v_{in}(t) = N_n \tau_a \frac{dv_{in}(t)}{dt} - \tau_b \frac{dv_{out}(t)}{dt}. \quad (14)$$

The NGD function operation can be rigorously realized under condition $|\tau_n| = 4T_s$. The discrete TF is designed by taking into account to the initial condition

$$v_{out}(0) = v_{in}(1) = v_{in}(0) = 0. \quad (15)$$

The LP-NGD function discretization is established from the differential infinitesimal elements, $dv_{in}(t)/dt$ and $dv_{out}(t)/dt$. By denoting the integer $k = 0, 1, 2, \dots, k_{max}$, we have the discrete quantities expressed as

$$\Delta v_{in}(kT_s)/\Delta t = [v_{in}(k+1) - v_{in}(k)]/T_s \quad (16)$$

$$\Delta v_{out}(kT_s)/\Delta t = [v_{out}(k+1) - v_{out}(k)]/T_s. \quad (17)$$

Substituting previous (16) and (17) into (14), the numerical LP-NGD difference equation can be fundamentally formulated by

$$v_{out}(k+1) = \zeta_2 v_{in}(k+1) + \zeta_1 v_{in}(k) + \zeta_0 v_{out}(k) \quad (18)$$

where

$$\begin{cases} \zeta_0 = \frac{\sqrt{4 + \omega_n^2 \tau_n^2} + \omega_n \tau_n}{\sqrt{4 + \omega_n^2 \tau_n^2} + \omega_n (\tau_n + 2T_s)} \\ \zeta_1 = \frac{N_n (\omega_n \tau_n - \sqrt{4 + \omega_n^2 \tau_n^2})}{\sqrt{4 + \omega_n^2 \tau_n^2} + \omega_n (\tau_n + 2T_s)} \\ \zeta_2 = \frac{N_n [\sqrt{4 + \omega_n^2 \tau_n^2} + \omega_n (2T_s - \tau_n)]}{\sqrt{4 + \omega_n^2 \tau_n^2} + \omega_n (\tau_n + 2T_s)} \end{cases}. \quad (19)$$

The LP-NGD infinite impulse response (IIR) coefficient variations are semi-logarithmically plotted in Fig. 5 for the particular case of NGD cutoff frequency-value product $\omega_n \tau_n = 2\pi$ or $f_n = 1/\tau_n$. As the present study is aimed to the NGD analysis with LF signal and high sampling rate, we choose the small range of NGD cutoff frequency-sampling rate period product $\omega_n T_s$ from 10^{-6} to 1. Coefficient ζ_0 is decreasing and the two other ones ζ_1 and ζ_2 increases with product $\omega_n T_s$.

It is worth noting that the initial value of the discrete variable allowing to realize a reasonable prediction must be

$$k_0 = Ent[\tau_n/T_s] \quad (20)$$

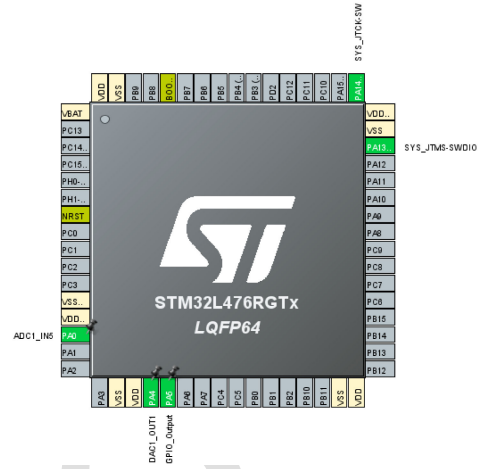


Fig. 6. STM32 MCU integrated circuit top view [37].

with $Ent[x]$ represents the superior integer part of real x .

As a validation, the innovative LP-NGD numerical function, original experimental results with STM32 MCU will be explored in the following section.

III. LP-NGD NUMERICAL FUNCTION EXPERIMENTATION WITH STM32 MCU

To verify the established numerical LP-NGD theory feasibility, a POC is designed via C-program code emulation driving an STM32 MCU board. This section presents the first NGD numerical experimental results based on the calculation and measurement comparison.

A. Description of the MCU-Based LP-NGD IIR Function

A Nucleo L476RG development board using an STM32L476RG MCU was used for this article [37]. The MCU package is 64-pin integrated circuit. Fig. 6 presents the top view of the employed STM32 MCU manufactured by STMicroelectronics [37] and the active pins needed to implement the LP-NGD TF. The MCU board is fed by $V_0 = 5$ V_{dc} power from USB connector. The microprocessor operating frequency is fixed at 80 MHz ADC are used in 12-bit precision.

The dynamic of operating input analog voltage can vary in the range between $V_{min} = 0$ V to $V_{max} = 3.3$ V with quantum resolution equal to $\Delta V = 800 \mu\text{V}$ under sampling frequency, $f_s = 5.33$ MHz. Then, the IIR NGD TF described in (18) is coded in C-language program, as indicated in Fig. 7.

During program execution, analog input voltage applied on pin PA0 is converted in a digital signal and processed. Output analog signal is delivered from pin PA5 through the DAC. During the operation test, the MCU configuration including the input and output signal interactions with the microprocessor is carried out by using the STM32CubeIDE software installed on the driver PC as described by the experimental test of the following section.

B. Numerical LP-NGD Experimental Setup

Fig. 8(a) highlights the real-time experimental setup of the STM32 MCU based IIR LP-NGD function. As indicated by

```

float zeta0 = 0.191; float zeta1 = -7.9; float zeta2 = 8.71;
float vin_1 = 0; float vin_0 = 0; float vout_1 = 0; float vout_0 = 0;
return float Process(float input)
{
//Update internally stored output at t-1
vout_1 = vout_0;
//Update internally stored input at t-1
vin_1 = vin_0;
//Update internally stored input at t
vin_0 = input;
//Compute output
vout_0 = zeta0*vout_0+ zeta1*vin_0+ zeta2*vin_1;
return vout_0;
}

```

Fig. 7. Numerical LP-NGD circuit code.

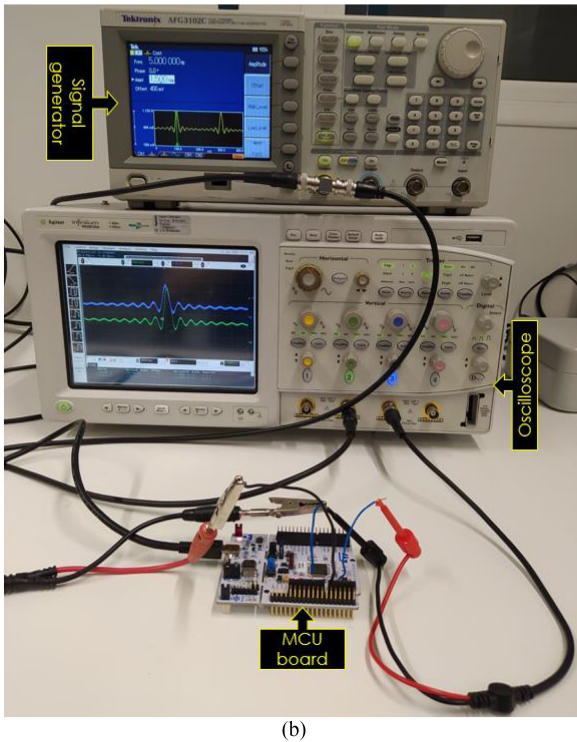
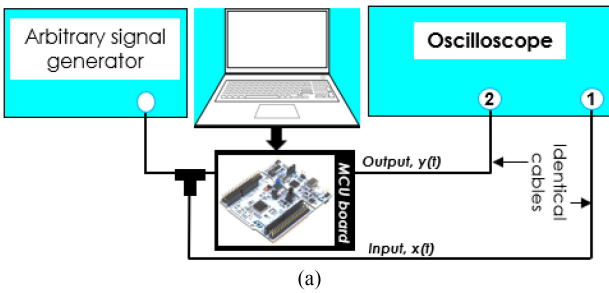


Fig. 8. (a) Illustrative diagram and (b) photograph of the LP-NGD MCU-based experimental setup.

TABLE I
TEST EQUIPMENT SPECIFICATIONS

| Description | Reference | Parameter | Value |
|------------------------------|---------------------------------|---------------|---------|
| Arbitrary function generator | Tektronix AFG3102C DUAL CHANNEL | Sampling rate | 1 GS/s |
| | | Bandwidth | 100 MHz |
| Digital oscilloscope | Agilent infiniium MSO8104A | V_{min} | 12.5 mV |
| | | Sampling rate | 4 GSa/s |
| | | Bandwidth | 1 GHz |
| | | Channels | 4 |

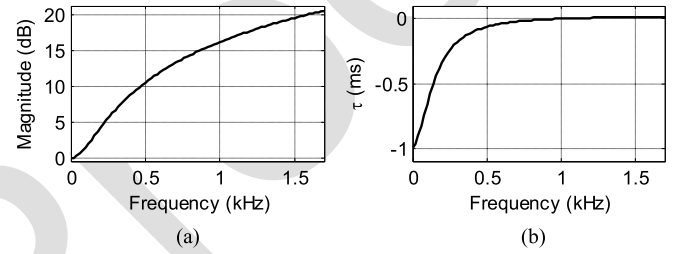


Fig. 9. LP-NGD frequency responses: (a) magnitude and (b) GD.

During the test, the oscilloscope input impedance is configured as $R_{in} = 1 \text{ } \Omega$. The employed test equipment specifications are addressed in Table I. Then, the tested signals are recorded in csv format and replotted in MATLAB environment. It is noteworthy that the MCU latency is about $21 \text{ } \mu\text{s}$.

C. Demonstration of Time < 0 Signal Prediction

This section discusses the demonstration results with three types of sensors. Prediction of arbitrary waveform signals in different time-scales is presented. The Gaussian pulse and sinc wave pulse signals were chosen for the LP-NGD time-domain validation because of the following reason.

- 1) They present a limited bandwidth, which can be assumed as the LP-NGD circuit cutoff frequency.
- 2) They enable to calculate the pulse duration in function of the LP-NGD circuit cutoff frequency.
- 3) To show the LP-NGD signature with the time-advance of leading- and tailing-edge between the input and output pulses.
- 4) To demonstrate the signal integrity by comparing the pulsewidth and amplitudes.
- 5) And to measure the magnitude effect by comparing the maximum peaks of input and output pulse signals.

1) LP-NGD Function Frequency Responses: Before the transient test, the LP-NGD circuit were synthesized under the desired specifications, static gain $N_0 = 0 \text{ dB}$, cutoff frequency $f_n = 1 \text{ kHz}$, and NGD value $\tau_n = -1 \text{ ms}$. Fig. 9 plots the magnitude and GD frequency responses from MATLAB computations of TF (5) in from dc to 1.7 kHz. These results confirm the LP-NGD behavior varying from -1 ms to 0 ms in the LF interval [0 Hz, 1 kHz] of the synthesized circuit. It is noteworthy that the gain at the cutoff frequency is approximately 17 dB. A limited bandwidth smoothed enough signal must be considered to realize the

Fig. 8(a), the input pulse analog voltage provided by the signal generator attacks the MCU and visualized simultaneously with the output analog voltage from pin PA5. The MCU is powered by USB port connected to the driver PC. Fig. 8(b) displays the photo of the performed experimental setup. As photographed by Fig. 8(b), the input and output analog signals are transmitted to the oscilloscope through a 1m-long cable.

TABLE II

SPECIFICATIONS OF THE INPUT GAUSSIAN SIGNALS, AND COMPARISON OF SIMULATED AND CALCULATED LP-NGD TRANSIENT SPECIFICATIONS

| Parameter | V_{max} | a | f_a | t_0 |
|-------------|-------------------|-------------------|--------|----------|
| Value | 1 V | 10 dB | 200 Hz | 8.9 ms |
| Approach | Δt_{rise} | Δt_{fall} | a | ϖ |
| Calculation | -0.58 ms | -1.26 ms | 1.05 | 92.7% |
| Measurement | -0.57 ms | -0.97 ms | 1.11 | 93.5% |

time-domain effect of the LP-NGD function. For this reason, the preliminary frequency domain analysis is necessary before the LP-NGD in the time-domain. To complete validation of the numerical LP-NGD function, time-domain measurement results will be examined in the following paragraph.

2) Time < 0 Demonstration With Numerical LP-NGD Gaussian Response: The LP-NGD transient analysis must be performed with smoothed signal presenting spectrum belonging to the NGD frequency band. Accordingly, the Gaussian waveform pulse as input test signal is analytically expressed as

$$v_{in}(t) = V_{max} e^{-(t-t_0)^2/\tau_a^2} \quad (21)$$

with maximal peak $V_{max} = v_{in}(t_0)$, at instant time t_0 , and spectrum bandwidth depending to the time parameter [38]

$$\tau_a = \sqrt{a_{dB} \ln(10)/5}/(\pi f_a) \quad (22)$$

where a_{dB} is the Gaussian spectrum attenuation at frequency f_a . Knowing the maximal instant time t_0 , the LP-NGD circuit transient characterization can be performed by rise-time advance $\tau_r = t_r^{out} - t_r^{in}$, and fall-time advance $\tau_f = t_f^{out} - t_f^{in}$, with $v_{in}(t_r^{in} < t_0) = \max[v_{in}(t)]/2$ and $v_{out}(t_r^{out} < t_0) = \max[v_{out}(t)]/2$, combined to voltage gain between the input and output signals

$$a = \max[v_{out}(t)] / \max[v_{in}(t)]. \quad (23)$$

And also, the input and output relative cross-correlation can be written as

$$\varpi(v_{in}, v_{out}) = \frac{\sum_{k=1}^{k_{max}} [v_{in}(k) - \hat{v}_{in}] [v_{out}(k) - \hat{v}_{out}]}{\sqrt{\sum_{k=1}^{k_{max}} [v_{in}(k) - \hat{v}_{in}]^2} \sqrt{\sum_{k=1}^{k_{max}} [v_{out}(k) - \hat{v}_{out}]^2}} \quad (24)$$

where the input and output average values, $\hat{v}_{in} = \sum_{k=1}^{k_{max}} v_{in}(k)/k_{max}$ and $\hat{v}_{out} = \sum_{k=1}^{k_{max}} v_{out}(k)/k_{max}$.

The transient calculation was carried out with Gaussian signal with $t_{max} = 20$ ms and different parameters indicated by Table II. During the calculation, the time step was fixed to 0.1 ms and the IIR coefficients defined in (20) are $\{\zeta_0 = 0.191, \zeta_1 = -7.9, \zeta_2 = 8.71\}$. Fig. 10(a) displays the comparison between the MATLAB modeled v_{out_C} (black dashed curve), and measured, v_{out_M} (red dashed curve), output signals of Gaussian input (blue solid curve) defined by (21). The tested LP-NGD IIR is defined by coefficients $\{\zeta_0 = 0.553, \zeta_1 = -22.91, \zeta_2 = 23.36\}$. For the present case of Gaussian response, considerable output uncontested time-advances are obtained for both leading- and tailing-edges. Based on this good correlation between model

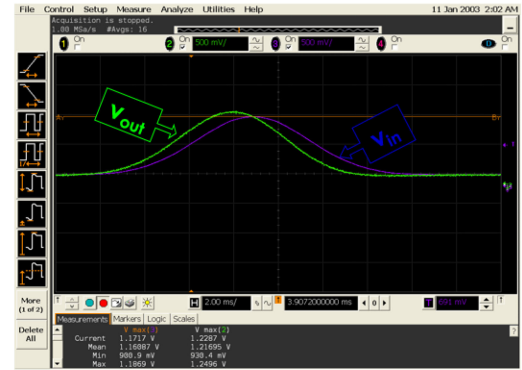
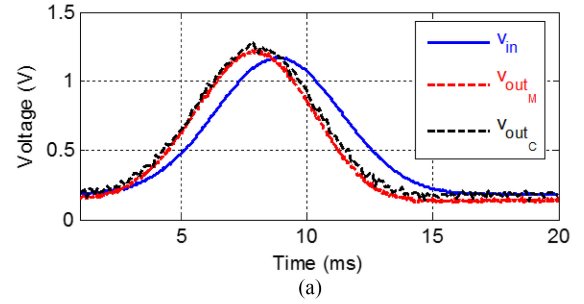


Fig. 10. (a) Calculated and measured LP-NGD MCU transient Gaussian pulse responses. (b) Corresponding oscilloscope screenshot of tested signals.

and measurement, the unfamiliar aspect of time advance is observed, which is a typical signature of LP-NGD function transient response. This sensational real-time result visualized by the screenshot Fig. 10(b) is the first time experimental and calculation validation of numerical LP-NGD circuit.

Moreover, Table II summarizes the LP-NGD transient characterization parameters. It is noteworthy that the numerical LP-NGD MCU input and output signal cross correlations are better than 92%.

The generality of the sensational time-advance was validated with two different arbitrary waveform and time-scale signals as explored in the following paragraphs.

3) Numerical LP-NGD Sinc Waveform Signal Response:

Another transient test of the LP-NGD numerical circuit was performed with 10-ms pulse duration and 1-V peak-to-peak amplitude sinc waveform. The considered sinc signal presents a frequency spectrum belonging into the NGD frequency band. Fig. 11(a) displays the comparison between the calculated v_{out_C} and measured v_{out_M} . Once again, the output signal time-advance was observed, as seen in the screenshot of Fig. 11(b). During the calculation, the time step was fixed to 0.1 ms. Once again, based on this result showing about -1 ms time advance average of output sinc leading and trailing edges, the STM32 MCU is able to operate as a LP-NGD numerical circuit. In this case, based on formula (24), measured and calculated output signals have a relative cross-correlation of about 89.3% and 87.7%. In addition to the signal generator input signal test, computational investigation with more industrial context of sensed arbitrary waveform signals plotted in several hours and very long-time duration is examined in the following paragraph.

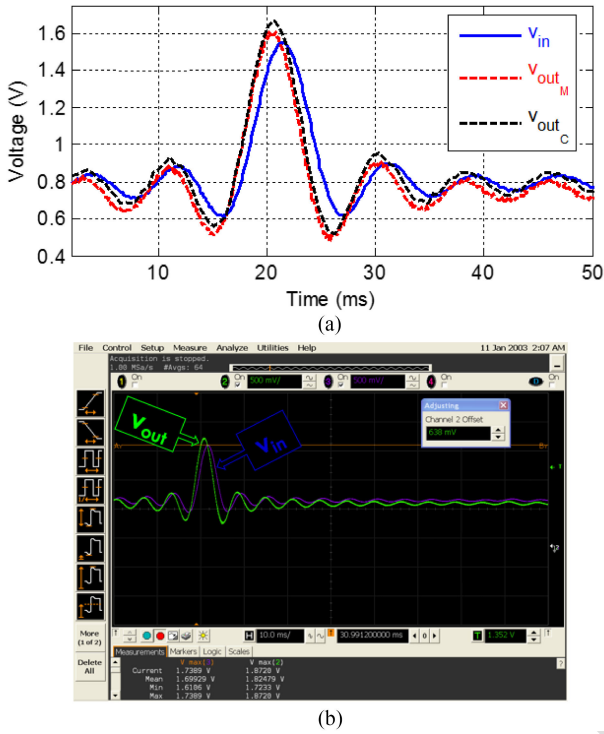


Fig. 11. (a) Calculated and measured LP-NGD MCU transient sinc waveform signal responses. (b) Corresponding oscilloscope screenshot of tested signals.

TABLE III

TEMPERATURE AND HUMIDITY WIRELESS SENSOR CHARACTERISTICS

| Measured parameter | Range | Accuracy | Type of sensor |
|--------------------|----------------|---------------------------------|--------------------|
| Temperature | -40°C to 125°C | +/- 0.4°C (max), at -10 to 85°C | Thermistor |
| Relative humidity | 0 to 100% | +/-3% (max), at 0 to 80% | Capacitive polymer |

4) Hour Time-Scale Arbitrary Sensored Signal Prediction

An illustrative industrial application case of LP-NGD function is described in this paragraph by using realm data recorded from temperature and humidity sensors. The realm data used in this paragraph were collected by sensors deployed on a student residence located in Douai city, in the north of France [39]. The adopted technology is wireless sensor network platforms based on a universal solution of the CLEODE company. Each smart-meter/device is set with a sampling time of $T_s = 2.4$ min, and its characteristics are given in Table III. Thus, these configurations allow us to monitor the external environment of buildings. Fig. 12 illustrate the evolution of the outdoor climate during the experimentation (from Feb. 9, 2019 to Feb. 21, 2019). On the top, we have the evolution of the outdoor temperature. That can take a value between 2 °C to 10 °C. In the bottom, we have the outdoor relative humidity. This last can take a value between 75% to 100%. In this case, the numerical LP-NGD function was synthesized under characteristics shown

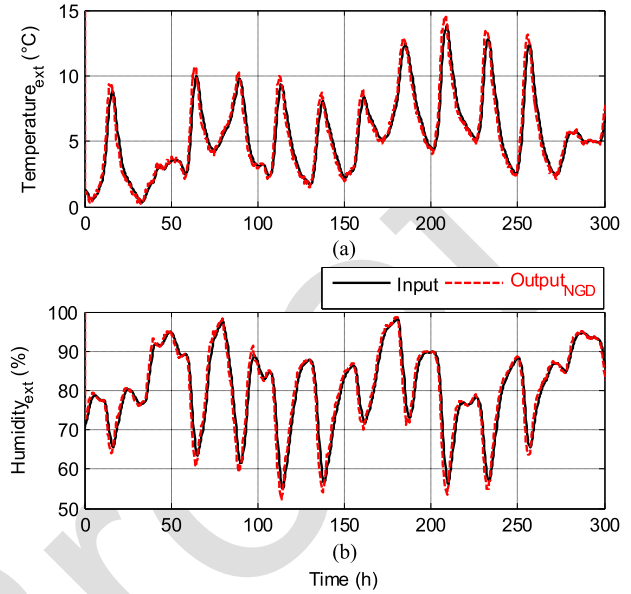


Fig. 12. LP-NGD responses of (a) temperature and (b) humidity sensors.

TABLE IV

NGD FUNCTION SPECIFICATIONS, AND TEMPERATURE AND HUMIDITY CROSS-CORRELATION

| Specifications | τ_n | f_n | ϖ |
|-------------------|----------|--------------|----------|
| Temperature | -1 h | 278 μ Hz | 81.8% |
| Relative humidity | | | 92.4% |

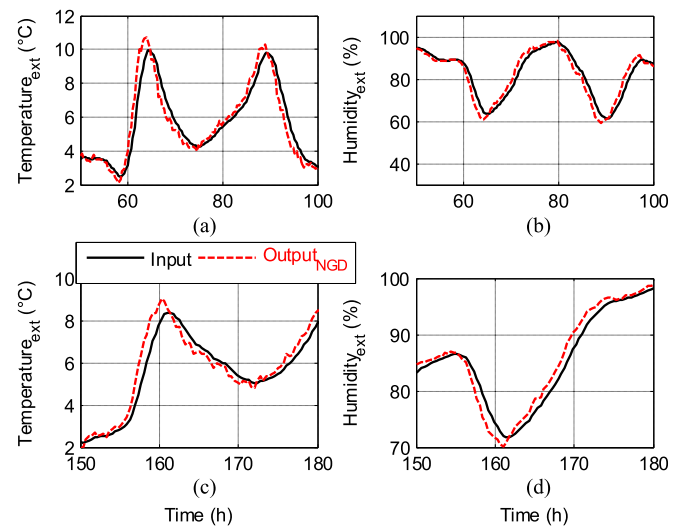


Fig. 13. Zoom in plots of LP-NGD responses of (a) [50 h, 100 h] and (b) [150 h, 180 h] time-interval temperature, and (c) [50 h, 100 h] and (d) [150 h, 180 h] time-interval humidity sensors.

in Table IV, $\tau_n = -3600$ s = -1 h and cutoff frequency, 390

$f_n = 278$ μ Hz. 391
The feasibility study is based 300 h (h) or 12.5 days duration 392
temperature and humidity measured sensed signals. The num- 393
erical LP-NGD computed responses are presented in Fig. 12(a) 394

and (b). The cross correlation between the input–output temperatures and humidity’s are 81.8% and 92.4%, as tabulated in Table IV, respectively. As illustrated by the time-domain results zoomed in time-intervals [50 h, 100 h] [see Fig. 13(a) and (c)], and [150 h, 180 h] [see Fig. 13(b) and (d)], an exciting result showing prediction of signal waveform is observed with output advance compared to the input under medium time-advance of about 1 h.

IV. CONCLUSION

The first-time investigation on design and test of LP-NGD numerical circuit was developed. The LP-NGD function was originally designed and emulated on STM32 MCU board [37]. An innovative theory of LP-NGD IIR TF was established. The main specifications of the input signal susceptible to operate with the LP-NGD function were defined in function of the MCU specifications. The design method and implementation of the numerical LP-NGD function was described. Then, the canonical fundamental discrete function of LP-NGD numerical circuit was analytically introduced. The LP-NGD analysis and synthesis methodology was originally formulated in function of the NGD specifications.

To validate the numerical LP-NGD function, an original experimental setup with STM32 MCU board was considered as a POC. The numerical LP-NGD circuit was experimentally validated by millisecond short-duration and computationally validated by hour long-duration arbitrary waveform signal testing. Results showed a very good agreement between the analytical computations and experimentations were introduced and discussed. The numerical LP-NGD function industrial application was promisingly highlighted by arbitrary waveform sensed signals representing temperature and humidity 12.5-day duration data from embedded sensors.

Compared with the traditional LP-NGD analog circuit, the investigated numerical NGD circuit presents.

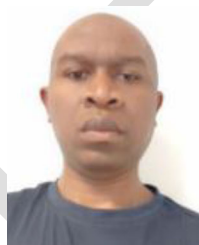
- 1) Benefits on i) the possibility to operate with long period signals having a duration of more than ten seconds (which cannot be treated with analog NGD circuits), ii) to interface the NGD circuit directly to digital signals, iii) to increase the order of LP-NGD circuit in order to widen the NGD bandwidth without increasing the physical size of the PCB prototype, and 4) to adjust negative delay programmatically according to the needs, making it versatile for a wide range of applications.
- 2) Disadvantages on i) the latency of the digital computations and ii) the delay introduced by ADC and DAC impacting the NGD response. However, especially for long NGD targeted by this digital implementation, conversion delays are usually negligible.

With this article, we envisage a revolution NGD technology for the future smart factories based on the sensed signal anticipation. To do this, the NGD MCU concept can be integrated in real-time simulation and deep learning interfaces [35], [36].

REFERENCES

- [1] A. Maiti, A. A. Kist, and A. D. Maxwell, “Real-time remote access laboratory with distributed and modular design,” *IEEE Trans. Ind. Electron.*, vol. 62, no. 6, pp. 3607–3618, Jun. 2015.
- [2] S. Liu, X. Wang, and P. X. Liu, “Impact of communication delays on secondary frequency control in an islanded microgrid,” *IEEE Trans. Ind. Electron.*, vol. 62, no. 4, pp. 2021–2031, Apr. 2015.
- [3] X. Lei, Y. Song, X. Yao, B. Dong, and M. Jin, “Effect of group delay on channel estimation performance in OFDM system,” *Appl. Math. Inf. Sci.*, vol. 6-3S, no. 3, pp. 1037–1045, 2012.
- [4] P.-Y. Chen, S. Yang, and J. A. McCann, “Distributed real-time anomaly detection in networked industrial sensing systems,” *IEEE Trans. Ind. Electron.*, vol. 62, no. 6, pp. 3832–3842, Jun. 2015.
- [5] N. Jalili and E. Esmailzadeh, “Optimum active vehicle suspensions with actuator time delay,” *Trans. ASME*, vol. 123, no. 1, pp. 54–61, Mar. 2001.
- [6] F. Wilches-Bernal *et al.*, “Effect of time delay asymmetries in power system damping control,” in *Proc. IEEE Power Energy Soc. Gen. Meeting*, Chicago, IL, USA, Jul. 16–20, 2017, pp. 1–5.
- [7] A. Pal, R. Kumar, and S. Das, “Stability and dynamic performance improvement of adaptive full-order observers in sensorless induction motor drives,” *Energy Procedia*, vol. 90, pp. 540–551, Dec. 2016.
- [8] A. B. Kahng and S. Muddu, “An analytical delay model of RLC interconnects,” *IEEE Trans. Comput.-Aided Des. Integrated Circuits Syst.*, vol. 16, no. 12, pp. 1507–1514, Dec. 1997.
- [9] R. Venkatesan, J. A. Davis, and J. D. Meindl, “Compact distributed RLC interconnect models - part IV: Unified models for time delay, crosstalk, and repeater insertion,” *IEEE Trans. Electron Devices*, vol. 50, no. 4, pp. 1094–1102, Apr. 2003.
- [10] S. Roy and A. Dounavis, “Efficient delay and crosstalk modeling of RLC interconnects using delay algebraic equations,” *IEEE Trans. Very Large Scale Integration*, vol. 19, no. 2, pp. 342–346, Feb. 2011.
- [11] B. Ravelo, “Delay modelling of high-speed distributed interconnect for the signal integrity prediction,” *Eur. Phys. J. Appl. Phys.*, vol. 57, Feb. 2012, Art. no. 31002.
- [12] Z. S. Veličković and V. D. Pavlović, “Complex analytic signals applied on time delay estimation,” *Phys., Chem. Technol.*, vol. 6, no. 1, pp. 11–28, 2008.
- [13] S.-S. Myoung, B.-S. Kwon, Y.-H. Kim, and J.-G. Yook, “Effect of group delay in RF BPF on impulse radio systems,” *IEICE Trans. Commun.*, vol. 90, no. 12, pp. 3514–3522, Dec. 2007.
- [14] G. Groenewold, “Noise and group delay in active filters,” *IEEE Trans. CAS I, Regular Papers*, vol. 54, no. 7, pp. 1471–1480, Jul. 2007.
- [15] L. Clifton, D. A. Clifton, M. A. F. Pimentel, P. J. Watkinson, and L. Tarassenko, “Predictive monitoring of mobile patients by combining clinical observations with data from wearable sensors,” *IEEE J. Biomed. Health Inform.*, vol. 18, no. 3, pp. 722–730, May 2014.
- [16] L. M. Nilsson, “Respiration signals from photoplethysmography,” *Anesthesia Analgesia*, vol. 117, no. 4, pp. 859–865, Oct. 2013.
- [17] J. L. Moraes, M. X. Rocha, G. G. Vasconcelos, J. E. Vasconcelos Filho, V. H. C. de Albuquerque, and A. R. Alexandria, “Advances in photoplethysmography signal analysis for biomedical applications,” *Sensors*, vol. 18, no. 6, pp. 1–26, Jun. 2018.
- [18] J. W. Chong *et al.*, “Photoplethysmograph signal reconstruction based on a novel hybrid motion artifact detection–reduction approach. Part I: Motion and noise artifact detection,” *Ann. Biomed. Eng.*, vol. 42, no. 11, pp. 2238–2250, Nov. 2014.
- [19] A. S. Junior, A. Spirandeli, R. Moraes, and V. Zarzoso, “Respiratory waveform estimation from multiple accelerometers: An optimal sensor number and placement analysis,” *IEEE J. Biomed. Health Inform.*, vol. 23, no. 4, pp. 1507–1515, Jul. 2019.
- [20] C. Hymel, R. A. Stubbers, and M. E. Brandt, “Temporally advanced signal detection: A review of the technology and potential applications,” *IEEE Circuits Syst. Mag.*, vol. 11, no. 3, pp. 10–25, Jul.–Sep. 2011.
- [21] H. U. Voss, “Signal prediction by anticipatory relaxation dynamics,” *Phys. Rev. E*, vol. 93, no. 3, 2016, Art. no. 030201R.
- [22] H. U. Voss and N. Stepp, “A negative group delay model for feedback-delayed manual tracking performance,” *J. Comput. Neurosci.*, vol. 41, no. 3, pp. 295–304, Dec. 2016.
- [23] K.-P. Ahn, R. Ishikawa, and K. Honjo, “Group delay equalized UWB ingap/gaas HBT MMIC amplifier using negative group delay circuits,” *IEEE Trans. Microw. Theory Techn.*, vol. 57, no. 9, pp. 2139–2147, Sep. 2009.

- [24] D. Solli, R. Y. Chiao, and J. M. Hickmann, "Superluminal effects and negative group delays in electronics, and their applications," *Phys. Rev. E*, vol. 66, 2002, Art. no. 056601.
- [25] F. Wan *et al.*, "Design of multi-scale negative group delay circuit for sensors signal time-delay cancellation," *IEEE Sensors J.*, vol. 19, no. 19, pp. 8951–8962, Oct. 2019.
- [26] M. W. Mitchell and R. Y. Chiao, "Causality and negative Group-delays in a simple bandpass amplifier," *Amer. J. Phys.*, vol. 66, no. 1, pp. 14–19, Nov. 1998.
- [27] M. W. Mitchell and R. Y. Chiao, "Negative Group-delay and 'Fronts' in a causal systems: An experiment with very low frequency bandpass amplifiers," *Phys. Lett. A*, vol. 230, no. 3/4, pp. 133–138, Jun. 1997.
- [28] T. Nakanishi, K. Sugiyama, and M. Kitano, "Demonstration of negative Group-delays in a simple electronic circuit," *Amer. J. Phys.*, vol. 70, no. 11, pp. 1117–1121, 2002.
- [29] M. Kitano, T. Nakanishi, and K. Sugiyama, "Negative Group-delay and superluminal propagation: An electronic circuit approach," *IEEE J. Sel. Topics Quantum Electron.*, vol. 9, no. 1, pp. 43–51, Feb. 2003.
- [30] B. Ravelo, "Similitude between the NGD function and filter gain behaviours," *Int. J. Circuit Theor. Appl.*, vol. 42, no. 10, pp. 1016–1032, Oct. 2014.
- [31] B. Ravelo, "First-order low-pass negative group delay passive topology," *Electron. Lett.*, vol. 52, no. 2, pp. 124–126, Jan. 2016.
- [32] F. Wan *et al.*, "Negative group delay theory of a four-port RC-Network feedback operational amplifier," *IEEE Access*, vol. 7, no. 1, pp. 75708–75720, Dec. 2019.
- [33] C. Kwan and R. Xu, "A note on simultaneous isolation of sensor and actuator faults," *IEEE Trans. Control Syst. Technol.*, vol. 12, no. 1, pp. 183–192, Jan. 2004.
- [34] N. Zhou, L. Luo, G. Sheng, and X. Jiang, "High accuracy insulation fault diagnosis method of power equipment based on power maximum likelihood estimation," *IEEE Trans. Power Del.*, vol. 34, no. 4, pp. 1291–1299, Aug. 2019.
- [35] Y. Chen and V. Dinavahi, "Hardware emulation building blocks for real-time simulation of large-scale power grids," *IEEE Trans. Ind. Inform.*, vol. 10, no. 1, pp. 373–381, Feb. 2014.
- [36] L. V. D. Maaten and G. Hinton, "Visualizing data using t-SNE," *J. Mach. Learn. Res.*, vol. 9, pp. 2579–2605, Nov. 2008.
- [37] ST, STM32L476xx, Datasheet-Production Data, pp. 1–270, Jun. 2019.
- [38] R. Vauche *et al.*, "High efficiency UWB pulse generator for ultra-low-power applications," *Int. J. Microw. Wireless Technol.*, vol. 8, no. 3, pp. 495–503, May 2016.
- [39] L. Rajaoarisoa, B. Ravelo, W. Rahajandraibe, and L. Etienne, "Weather prediction to improve energy efficiency and climate control of the buildings," in *Proc. IBPSA France*, Nov. 12/13, 2020, pp. 1–7.



Blaise Ravelo (Member, IEEE) is currently a University Full Professor with the Nanjing University of Information Science and Technology, Nanjing, China. His research interests include on multiphysics and electronics engineering.

Prof. Ravelo is a Pioneer of the Negative Group Delay (NGD) concept about $t < 0$ signal travelling physical space. He was research director of 11 Ph.D. students (eight defended), postdocs, research engineers, and Master internships. With US, Chinese, Indian, European, and African partners, he is actively involved and contributes on several international research projects (ANR, FUI, FP7, INTERREG, H2020, Euripides², Eurostars...). He is Member of IET Electronics Letters Editorial Board as Circuit and System Subject Editor. He is ranked in Top 2% world's scientists based on years 2019 by Stanford University, US. He has Google scholar h-index (2021) = 23 and i10-index(2021) = 68. He is member of research groups: IEEE, URSI, GDR Ondes, Radio Society and (co-) authors of more than 360 scientific research papers in new technologies published in International Conference and Journals. He is Lecturer on Circuit and System Theory, STEM (science, technology, engineering, and maths) and applied physics. He is regularly invited to review papers submitted for publication to international journals (IEEE TRANSACTIONS ON MICROWAVE THEORY AND TECHNIQUES, IEEE TRANSACTIONS ON CIRCUITS AND SYSTEMS, IEEE TRANSACTIONS ON ELECTROMAGNETIC COMPATIBILITY, IEEE TRANSACTIONS ON INDUSTRIAL ELECTRONICS, IEEE ACCESS, *IET Circuits, Devices, and Systems*, and *IET Microwaves, Antennas and Propagation*) and books (Wiley, Intech Science).



Mathieu Guerin (Member, IEEE) received the Engineering degree in microelectronics and telecommunications from Polytech Marseille, Marseille, France, and the Research Master degree in integrated circuits design from the University of Aix-Marseille, Marseille, France, both in 2010, and the doctorate degree from the University of Aix-Marseille, in 2010.

He was a Technical Leader of the Analog and Radio-Frequency Design Team of IDEMIA-StarChip for five years and designed chips embedded in SIM cards and contactless bank cards with biometric recognition. He joined Aix-Marseille University as an Assistant Professor in 2020 and joined the CCSI Team of the IM2NP Laboratory. He is working on methods of modeling and characterizing circuits in analog electronics. His research interest includes the design and synthesis of circuits in digital electronics.



Wencelias Rahajandraibe (Member, IEEE) received the B.Sc. degree in electrical engineering from Nice Sophia-Antipolis University, Nice, France, in 1996, the M.Sc. degree (with distinction) in electrical engineering from the Science Department, University of Montpellier, Montpellier, France, in 1998, and the Ph.D. degree in microelectronics from the University of Montpellier.

He is currently a Full Professor with the University of Aix-Marseille, Marseille, France. Since 1998, he has been with the Microelectronics Department of Informatics, Robotics and Microelectronics, Laboratory of Montpellier (LIRMM). Since 2003, he has been with the Microelectronic Department of Materials, Microelectronics and Nanoscience, Laboratory of Provence (IM2NP), Marseille, France, where he was an Associate Professor. Since 2014, he has been a Professor with Aix Marseille University where he heads the Integrated Circuit Design group of the IM2NP Laboratory. He is regularly involved to participate and to lead national and international research projects (ANR, H2020, FP7 KIC-InnoEnergy...). He directed and cosupervised 18 Ph.D. and 15 Master students. He has authored or coauthored 11 patents and more than 150 papers published in refereed journals and conferences. His research interests include AMS and RF circuit design from transistor to architectural level. His current research interests include ultralow power circuit design for smart sensor interface and embedded electronic in bioelectronic and e-health applications, wireless systems, design technique, and architecture for multistandard transceiver.

Prof. Rahajandraibe is an Expert for the ANR, the French Agency for Research. He has served on program committees of IEEE INTERNATIONAL NEW CIRCUITS AND SYSTEMS CONFERENCE and IEEE INTERNATIONAL CONFERENCE ON ELECTRONICS, CIRCUITS, AND SYSTEMS. He has been and is a Reviewer of contributions submitted to several IEEE conferences and journals such as IEEE INTERNATIONAL SYMPOSIUM ON CIRCUITS AND SYSTEMS, IEEE INTERNATIONAL NEW CIRCUITS AND SYSTEMS CONFERENCE, IEEE INTERNATIONAL MIDWEST SYMPOSIUM ON CIRCUITS AND SYSTEMS, ESSCIRC, ESSDERC, RFIC, IEEE TRANSACTIONS ON CIRCUITS AND SYSTEMS I AND II, *IET Electronics Letters*.



Valentin Gies (Member, IEEE) received the Graduate degree in applied physics from Ecole Normale Supérieure, Paris, France, in 2001, and the Ph.D. degree in electronics from Ecole Nationale Supérieure de Techniques Avancées, Paris XI Orsay University, Orsay, France, in 2005.

His Ph.D. was focused on both circuits and algorithms for artificial Retinas. He is Lecturer and Researcher with Toulon University since 2007, and an Associate Professor in Robotics, Embedded Electronics and IoT at SeaTech, ISEN Toulon, and ENSTA ParisTech. He was with the IM2NP CNRS Laboratory in 2017, in the Circuits Design Team. His current research interests include embedded algorithms and circuits for ultralow power systems.

Prof. Gies is Scientific Advisor of several start-ups in IoT and Head of Scientific Microsystems for Internet of Things, Toulon University.

Q5
Q6

Q7

Q3

Q4

670
671
672
673
674
675
676
677
678
679
680
681
682
683
684
685
686
687
688
689
690



Lala Rajoarisoa (Member, IEEE) received the M.Sc. and Ph.D. degree in automatic and computer sciences from the University of Aix-Marseille, Marseille, France, in 2005 and 2009, respectively.

He is currently an Assistant Professor with the Institut Mines-Télécom Lille Douai. Develop predictive models and controllers to assess system behavior and optimize its performance. This development includes the analysis of intrinsic properties such as stability, observability, identifiability, and controllability. He is involved in research activities dedicated to the optimization of energy efficiency of building systems and the control and management of hydraulic systems with more than 80 papers published in refereed journals and conferences. He regularly participates and contributes on several international projects (ANR, FUI, and INTERREG) and was the supervisor of more than of 15 Ph.D. students, postdocs, research engineers, and Master internships. His research interests include the development of data-driven tools and methods for the observation and control of large-scale distributed systems.



Sébastien Lalléchère (Member, IEEE) was born in Nevers, France, in 1979. He received the M.Sc. and Ph.D. degrees in computational modeling and electronics/electromagnetism from Polytech Clermont and Université Blaise Pascal, Clermont-Ferrand, France, in 2002 and 2006, respectively.

He was Research Engineer with LASMEA, Clermont-Ferrand, France, in 2007 focusing on intensive computational methods for electromagnetics. He is currently an Associate Professor with the Institut Pascal and Université Clermont Auvergne, Clermont-Ferrand, France. His research interests include electromagnetic compatibility including antennas and propagation, complex and reverberating electromagnetic environments, electromagnetic coupling, computational electromagnetics, stochastic modeling, and sensitivity analysis in electrical engineering.

691
692
693
694
695
696
697
698
699
700
701
702
703
704
705
706
707
708

IEEE PROCEEDINGS

GENERAL INSTRUCTION

- **Authors:** Carefully check the page proofs (and coordinate with all authors); additional changes or updates **WILL NOT** be accepted after the article is published online/print in its final form. Please check author names and affiliations, funding, as well as the overall article for any errors prior to sending in your author proof corrections.
- **Authors:** We cannot accept new source files as corrections for your article. If possible, please annotate the PDF proof we have sent you with your corrections and upload it via the Author Gateway. Alternatively, you may send us your corrections in list format. You may also upload revised graphics via the Author Gateway.
- **Authors:** Unless invited or otherwise informed, there is a mandatory Excessive Article Length charge of \$250 per page (\$200 for IES members) in excess of eight (8) pages. If you have any questions regarding overlength page charges, need an invoice, or have any other billing questions, please contact apcinquries@ieee.org as they handle these billing requests.

QUERIES

- Q1. Author: Please provide the expansion for the acronym DAC.
- Q2. Author: Please provide the ORCID for the corresponding author Mathieu Guerin.
- Q3. Author: Please update the Ref. [37]
- Q4. Author: Please provide the educational details (degree/university/location/subject) for author Blaise Ravelo.
- Q5. Author: Please check whether the biography of author Mathieu Guerin is correct as set.
- Q6. Author: Please provide the subject in which the author Mathieu Guerin received the doctorate degree.
- Q7. Author: Please provide the year in which the author Wenceslas Rahajandraibe received the Ph.D. degree.

Low-Pass NGD Numerical Function and STM32 MCU Emulation Test

Blaise Ravelo ¹, Member, IEEE, Mathieu Guerin, Member, IEEE,
Wenceslas Rahajandraibe ², Member, IEEE, Valentin Gies, Member, IEEE,
Lala Rajaoarisoa ³, Member, IEEE, and Sébastien Lalléchère ⁴, Member, IEEE

Abstract—This article introduces an original microcontroller unit (MCU) design of numerical low-pass (LP) negative group delay (NGD) function. The innovative theory of the numerical LP-NGD function is developed based on the first-order analog transfer function discretization. The infinite impulse response (IIR) LP-NGD is fundamentally formulated in function of the desired NGD value, cutoff frequency, gain, and the MCU sampling frequency. A STM32 MCU proof-of-concept (POC) is tested to implement the IIR LP-NGD function. Different real-time tests with visualization of input and output analog signals from the MCU LP-NGD POC were performed. As expected, time-advance demonstration tests with milli-second short- and several hour long-duration time-scale with arbitrary waveform signals from temperature and humidity sensors. The signal time-advance is not in contradiction with the causality. The proposed digital MCU function opens a potential future industrial application of LP-NGD function via sensed signal anticipation.

Index Terms—Circuit design, emulation, microcontroller unit (MCU), negative group delay (NGD), numerical circuit, time-domain demonstration.

I. INTRODUCTION

IN EARLY age of Industry 4.0 revolution, the role of remote communication is one of the design research engineer breakthrough [1]. The delay effect plays a major role on the communication system general performance [2]–[4]. For example, these effects are critical for reliable operation of remote-control

Manuscript received March 29, 2021; revised June 17, 2021 and July 3, 2021; accepted August 23, 2021. (Corresponding author: Mathieu Guerin.)

Blaise Ravelo is with the Nanjing University of Information Science and Technology, Nanjing 210044, China (e-mail: blaise.ravelo@yahoo.fr).

Mathieu Guerin, Wenceslas Rahajandraibe, and Valentin Gies are with the CNRS, University of Toulon, 83130 Marseille, France, and also with the Aix-Marseille University, 3007 Marseille, France (e-mail: mathieu.guerin@im2np.fr; wenceslas.rahajandraibe@im2np.fr; valentin.gies@im2np.fr).

Lala Rajaoarisoa is with the IMT Lille Douai, Institut Mines-Télécom, Centre for Digital Systems, University Lille, F-59000 Lille, France (e-mail: lala.rajaoarisoa@imt-lille-douai.fr).

Sébastien Lalléchère is with the Institute Pascal, SIGMA Clermont, Université Clermont Auvergne, 63001 Clermont Ferrand, France (e-mail: sebastien.lallechere@uca.fr).

Color versions of one or more figures in this article are available at <https://doi.org/10.1109/TIE.2021.3109543>.

Digital Object Identifier 10.1109/TIE.2021.3109543

system. The quality of service (QoS) of remote sensing systems forecasted Industry 4.0 factories to operate correctly depends undeniably on the delay effects. The networked modern industrial sensing systems present an open risk of anomaly detection because of unintentional delays. So far, no rigorous solution is available to overcome the time delay effects in almost all areas of engineering [2]–[9].

One can cite different challenges to be overcome to face up the delay impacts. The signal delay degrades the digital communication QoS due to the wireless propagation channel dispersion and data desynchronization [3]–[4]. In the area of automation and control engineering, different industrial application examples as optimal vehicle activities [5], networked control system, and power system damping control [6] present performance limitations because of the delay effect. Time-domain analyses confirm that the stability of dynamic systems depend unavoidably to the feedback delays [7].

To take into account the delay effects on the system performance, analytical, and modeling methods for the enhancement of printed circuit board (PCB) signal integrity were proposed [8]–[11]. Delay estimation techniques were developed for estimating communication system performance [3]. Diverse estimation techniques based on complex analytical signals [12] have been developed. In addition to the noise effect issues, the group delay (GD) limits undesirably the communication performances [13]–[14].

In the area of biomedical engineering, under the telemedicine revolution, new generation of wearable biosensors is currently developed [15]. The delay effects play also a vital role on the performance of the wearable sensor signal monitoring. An innovative photoplethysmography signal measurements of respiration, oxygen, and blood pressure rate measurement were proposed [16]–[18]. A technique allowing to use an optimal number and positioning of multiple accelerometers for respiratory waveform estimation is developed in [19]. To improve the medical sensor performances, an advanced signal detection technique using negative GD (NGD) function is developed in [20]. Under the same challenge, an NGD predictor based on anticipatory relax dynamics using basically a delayed induced feedback function is proposed in [21] and [22].

In electronics engineering, NGD microwave monolithic integrated circuits have been employed to equalize the undesirable signal degradations as regularly found in the PCBs [23]. This NGD equalization technique was initiated in [24] for RC-effect

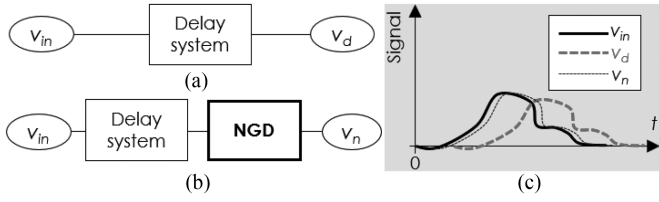


Fig. 1. Illustration scenario of NGD application. (a) Delay penalizing system. (b) NGD corrected system. (c) Input and output signal chronogram.

and to cancel out the signal delay. Fig. 1 illustrates a scenario of signal delay cancellation NGD application with delay system. Because of the NGD function, the delay between input signal v_{in} and output signal v_d is larger than that of v_{in} and v_n [$\text{delay}(v_{in}, v_d) \gg \text{delay}(v_{in}, v_n)$].

The technique was introduced in [25] to target industrial applications by overcoming multisensor time-delays. Acting as an unfamiliar function, it is worth to define what is the NGD function meaning. To answer to this curiosity, a brief state of the art about the NGD function will be described in the following paragraph.

The NGD phenomenon was initially validated with low-frequency (LF) electronic circuits in 1990s [26], [27]. Despite the counterintuitive aspect, the NGD circuits can be designed and implemented like classical and familiar electrical circuits as filters, amplifiers, phase shifters, oscillators. The LF NGD topologies proposed initially in [26]–[29] were built with classical electronic passive (R, L, and C) and operational amplifier components. The NGD phenomenon meaning was illustrated with time-domain experimentations showing the possibility to propagate the NGD output signal in time-advance with the input one [26]–[29]. This demonstration was realized with PCB showing an NGD output lamp lightened on before the input one [29]. This counterintuitive NGD phenomenon is not in contradiction with the causality principle [26]–[29]. For further understanding about the NGD concept, an investigation on the similitude between the NGD and linear filter gain behaviors is introduced in [30]. The concept of low-pass (LP) [31], [32] NGD function was initiated. Despite the research work progress in the area of electronics engineering, the NGD function remains an unmaturing concept for most of industrial engineers. Open questions are regularly asked about the industrial potential applications of the NGD function.

For this reason, a completely original research work on the design of numerical LP NGD circuit is developed in the present paper. The LP-NGD function is implemented on microcontroller unit (MCU) operating in different time scales. The NGD function can be potentially used as a pioneer work of anticipator for the real-time predetection of actuator and sensor faults and intelligent system diagnoses [33], [34]. The research work originality relies on the MCU numerical LP-NGD function design and test. For the better understanding, this paper is organized in three main sections. Section II will describe the numerical LP-NGD transfer function (TF) theory. Section III will present the LP-NGD MCU demonstrator as proof-of-concept (POC). Finally, Section IV concludes this article.

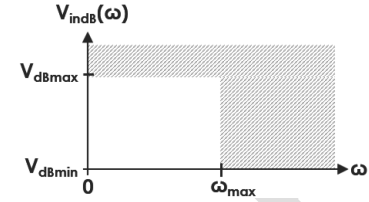


Fig. 2. Specific characterization diagram of numerical LP-NGD input signal.

II. MCU DESIGN PRINCIPLE OF DISCRETE LP NGD FUNCTION

Acting as one of the most unfamiliar digital function available in the literature, it would be necessary to define the operating input signal specifications before the theorization of the discrete LP-NGD TF.

A. Input Signal and MCU Specifications

A LP-NGD function is dedicated to operate with base band signal, which can be noticed by v_{in} . The ideal specifications of its frequency spectrum magnitude in dB of $V_{in}(j\omega)$ are illustrated in Fig. 2 by denoting the angular frequency variable ω . In this diagram, the signal spectrum magnitude is assumed $V_{in} = 0$ in the forbidden zone represented by the shadowed area. Signal v_{in} can present any arbitrary waveform but should be limited bandwidth denoted ω_{max} . The signal minimal and maximal strengths, denoted by V_{min} and V_{max} , need to be defined.

The MCU architecture is assumed powered by $V_{dd} = V_0$. It is mainly constituted by the block of computing core interfaced by analog digital converters (ADC) and DAC as input and output interfaces, respectively. The MCU operation is cadenced by its internal clock generating the sampling clock supposed with period denoted $T_s = 1/f_s$ (f_s is the sampling frequency). Given the case of input signal duration t_{max} , the MCU must operate with time step following the integer index $k = 0, 1, 2, \dots, k_{max} = \text{Ent}[t_{max}/T_s]$ by denoting $\text{Ent}[x]$ the superior integer part of real positive x . The discrete input and output signals at the instant time $t = kT_s$ are represented by

$$\begin{cases} v_{in}(k) = v_{in}(kT_s) \\ v_{out}(k) = v_{out}(kT_s) \end{cases} \quad (1)$$

B. Theoretical Investigation of Discrete LP-NGD Function

This section describes the main specifications and characterization of numerical LP-NGD function.

1) NGD Specifications: The NGD TF can be represented as a single-input single-output block diagram, as shown in Fig. 3(a). With the Laplace variable s , the associated analog TF can be formulated by $N(s) = V_{out}(s)/V_{in}(s)$. The NGD analysis in the frequency domain is based on the consideration of magnitude response, $N(\omega) = |N(j\omega)|$ and the GD defined by

$$\tau(\omega) = -\partial\varphi(\omega)/\partial\omega \quad (2)$$

with

$$\varphi(\omega) = \arctan \{ \text{Im} [N(j\omega)] / \text{Re} [N(j\omega)] \}. \quad (3)$$

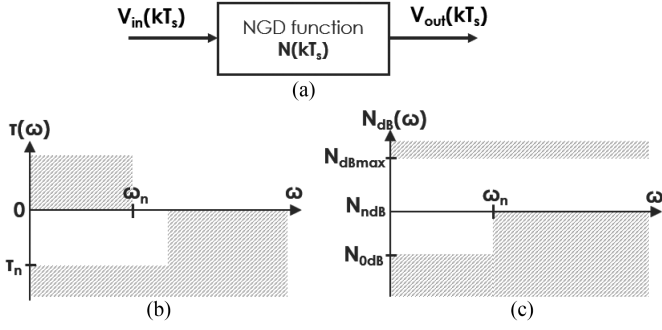


Fig. 3. (a) Block, (b) GD, and (c) magnitude response diagrams of LP-NGD function.

Fig. 3(b) represents the GD diagram specific to the ideal LP-NGD function, which is defined by two fundamental characteristics as follows.

- 1) The NGD value at very low frequencies

$$\tau_n = \tau(\omega \approx 0) < 0. \quad (4)$$

- 2) The NGD cutoff angular frequency $\omega_n = 2\pi f_n$, which is a root of the equation $\tau(\omega) = 0$.

Fig. 3(c) highlights the LP-NGD magnitude response specifications. For the case of first order linear NGD system (which will be explored in the following paragraph), it associates three main characteristics.

- 3) The minimal magnitude $N_{dBmin} = N_{0dB} = N_{dB}(\omega \approx 0)$, which should correspond to the magnitude at very LFs.
- 4) The maximal magnitude $N_{dBmax} = N_{dB}(\omega \approx \infty)$, which should be reached at very high frequencies.
- 5) And the magnitude $N_{ndB} = N_{dB}(\omega = \omega_n)$ at cutoff frequency.

2) Canonical Form of First Order LP-NGD TF: With the real parameters defined previously N_n , τ_n , and ω_n , the canonical form of LP-NGD analog TF is defined as [31]

$$N(s) = N_n(1 + \tau_a s)/(1 + \tau_b s) \quad (5)$$

where

$$\tau_a = \left(\sqrt{\tau_n^2 + 4/\omega_n^2} - \tau_n \right) / 2 \quad (6)$$

$$\tau_b = \left(\sqrt{\tau_n^2 + 4/\omega_n^2} + \tau_n \right) / 2. \quad (7)$$

The integrity between NGD input and output signals, v_{in} and v_{out} can be quantified with the quantity $M_n = N(\omega_n)$. The LP-NGD bandwidth magnitude flatness and maximal flatness factor can be assessed by the ratio, respectively, as follows:

$$\xi(\varpi) = M_n(\varpi)/N_n \quad (8)$$

$$\xi_{max}(\varpi) = N_{max}(\varpi)/N_n \quad (9)$$

where the NGD value-bandwidth product

$$\varpi = -\omega_n \tau_n. \quad (10)$$

By considering the LP-NGD TF expressed in (5), the previous magnitude flatness factors are rewritten as

$$\xi(\varpi)$$

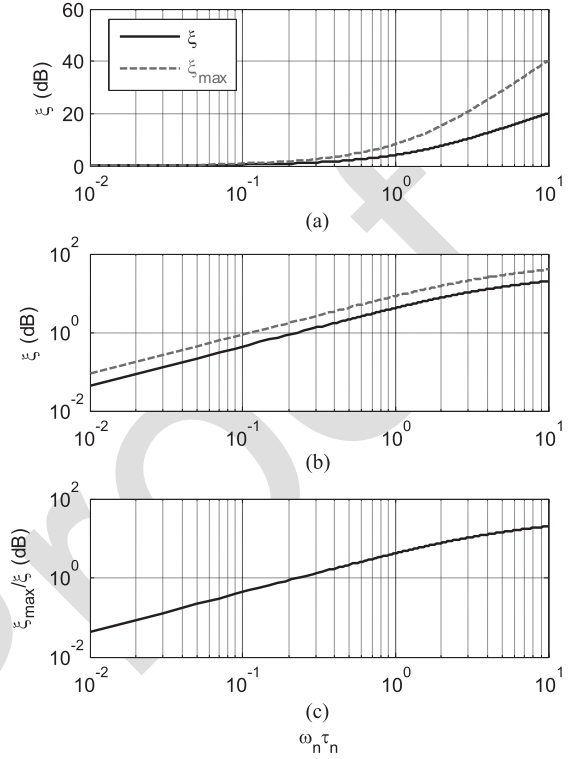


Fig. 4. LP-NGD TF magnitude flatness versus product $\omega_n \tau_n$ in (a) semilog x-axis, (b) log-log plots, and (c) ratio from (9).

$$= \left[\sqrt{4 + (\sqrt{\varpi^2 + 4} + \varpi)^2} \right] / \left[\sqrt{4 + (\sqrt{\varpi^2 + 4} - \varpi)^2} \right] \quad (11)$$

$$\xi_{max}(\varpi) = (\sqrt{\varpi^2 + 4} + \varpi) / (\sqrt{\varpi^2 + 4} - \varpi). \quad (12)$$

3) Characterization of LP-NGD TF Flatness: The magnitude flatness constitutes one of the main parameters affecting the LP-NGD function performance. It is particularly important to investigate the LP-NGD TF magnitude variation range in the NGD frequency band. Following this point, we considered the general plot of the flatness defined by (11). Fig. 4 displays the plots of these magnitude flatness factors in function of the NGD value-bandwidth product varied from 0.01 to 10. The flatness differences varied from 0 to 19 dB and we have $N_{max}/N_n > 1$ because $\tau_n < 0$.

C. LP-NGD Numerical Function Expression

The original numerical LP-NGD function is originally elaborated from the first-order LP-NGD canonical TF given in (5). Indeed, the TF equivalent discrete form is derived from the equivalent differential equation governing input v_{in} and output v_{out} . To realize the time-advance behavior related to the LP-NGD function, the input signal bandwidth should respect condition $\omega_{max} \leq \omega_n$. The analytical combination of $N(s)$ definition and TF (5) implies the Laplace symbolic equation

$$V_{out}(s) - N_n V_{in}(s) = s [N_n \tau_a V_{in}(s) - \tau_b V_{out}(s)]. \quad (13)$$

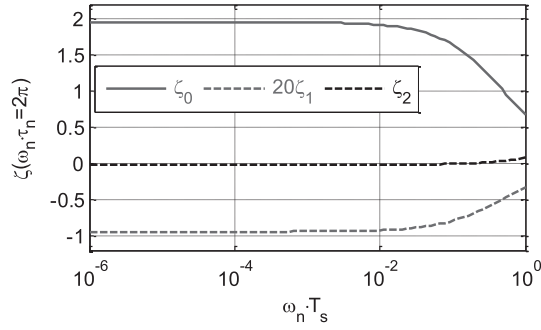


Fig. 5. Variations of LP-NGD IIR coefficients versus product $\omega_n T_s$.

By supposing that the input signal is generated under the initial condition $v_{in}(t = 0) = 0$. It can be derived with Laplace inverse transform the time-dependent differential equation

$$v_{out}(t) - N_n v_{in}(t) = N_n \tau_a \frac{dv_{in}(t)}{dt} - \tau_b \frac{dv_{out}(t)}{dt}. \quad (14)$$

The NGD function operation can be rigorously realized under condition $|\tau_n| = 4T_s$. The discrete TF is designed by taking into account to the initial condition

$$v_{out}(0) = v_{in}(1) = v_{in}(0) = 0. \quad (15)$$

The LP-NGD function discretization is established from the differential infinitesimal elements, $dv_{in}(t)/dt$ and $dv_{out}(t)/dt$. By denoting the integer $k = 0, 1, 2, \dots, k_{max}$, we have the discrete quantities expressed as

$$\Delta v_{in}(kT_s)/\Delta t = [v_{in}(k+1) - v_{in}(k)]/T_s \quad (16)$$

$$\Delta v_{out}(kT_s)/\Delta t = [v_{out}(k+1) - v_{out}(k)]/T_s. \quad (17)$$

Substituting previous (16) and (17) into (14), the numerical LP-NGD difference equation can be fundamentally formulated by

$$v_{out}(k+1) = \zeta_2 v_{in}(k+1) + \zeta_1 v_{in}(k) + \zeta_0 v_{out}(k) \quad (18)$$

where

$$\begin{cases} \zeta_0 = \frac{\sqrt{4 + \omega_n^2 \tau_n^2} + \omega_n \tau_n}{\sqrt{4 + \omega_n^2 \tau_n^2} + \omega_n (\tau_n + 2T_s)} \\ \zeta_1 = \frac{N_n (\omega_n \tau_n - \sqrt{4 + \omega_n^2 \tau_n^2})}{\sqrt{4 + \omega_n^2 \tau_n^2} + \omega_n (\tau_n + 2T_s)} \\ \zeta_2 = \frac{N_n [\sqrt{4 + \omega_n^2 \tau_n^2} + \omega_n (2T_s - \tau_n)]}{\sqrt{4 + \omega_n^2 \tau_n^2} + \omega_n (\tau_n + 2T_s)} \end{cases}. \quad (19)$$

The LP-NGD infinite impulse response (IIR) coefficient variations are semi-logarithmically plotted in Fig. 5 for the particular case of NGD cutoff frequency-value product $\omega_n \tau_n = 2\pi$ or $f_n = 1/\tau_n$. As the present study is aimed to the NGD analysis with LF signal and high sampling rate, we choose the small range of NGD cutoff frequency-sampling rate period product $\omega_n T_s$ from 10^{-6} to 1. Coefficient ζ_0 is decreasing and the two other ones ζ_1 and ζ_2 increases with product $\omega_n T_s$.

It is worth noting that the initial value of the discrete variable allowing to realize a reasonable prediction must be

$$k_0 = Ent[\tau_n/T_s] \quad (20)$$

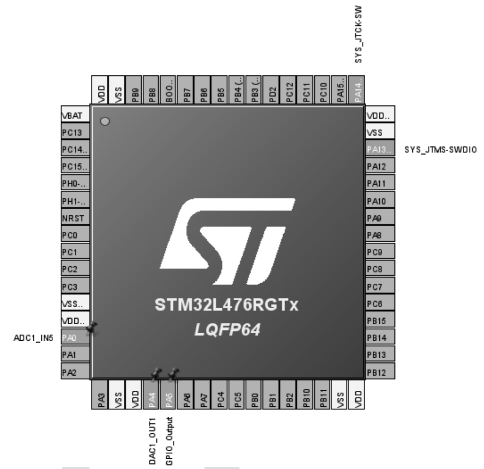


Fig. 6. STM32 MCU integrated circuit top view [37].

with $Ent[x]$ represents the superior integer part of real x .

As a validation, the innovative LP-NGD numerical function, original experimental results with STM32 MCU will be explored in the following section.

III. LP-NGD NUMERICAL FUNCTION EXPERIMENTATION WITH STM32 MCU

To verify the established numerical LP-NGD theory feasibility, a POC is designed via C-program code emulation driving an STM32 MCU board. This section presents the first NGD numerical experimental results based on the calculation and measurement comparison.

A. Description of the MCU-Based LP-NGD IIR Function

A Nucleo L476RG development board using an STM32L476RG MCU was used for this article [37]. The MCU package is 64-pin integrated circuit. Fig. 6 presents the top view of the employed STM32 MCU manufactured by STMicroelectronics [37] and the active pins needed to implement the LP-NGD TF. The MCU board is fed by $V_0 = 5$ V_{dc} power from USB connector. The microprocessor operating frequency is fixed at 80 MHz ADC are used in 12-bit precision.

The dynamic of operating input analog voltage can vary in the range between $V_{min} = 0$ V to $V_{max} = 3.3$ V with quantum resolution equal to $\Delta V = 800 \mu\text{V}$ under sampling frequency, $f_s = 5.33$ MHz. Then, the IIR NGD TF described in (18) is coded in C-language program, as indicated in Fig. 7.

During program execution, analog input voltage applied on pin PA0 is converted in a digital signal and processed. Output analog signal is delivered from pin PA5 through the DAC. During the operation test, the MCU configuration including the input and output signal interactions with the microprocessor is carried out by using the STM32CubeIDE software installed on the driver PC as described by the experimental test of the following section.

B. Numerical LP-NGD Experimental Setup

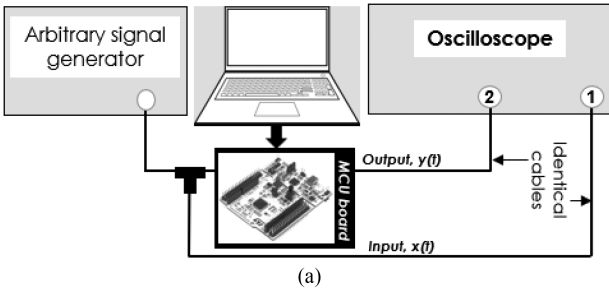
Fig. 8(a) highlights the real-time experimental setup of the STM32 MCU based IIR LP-NGD function. As indicated by


```

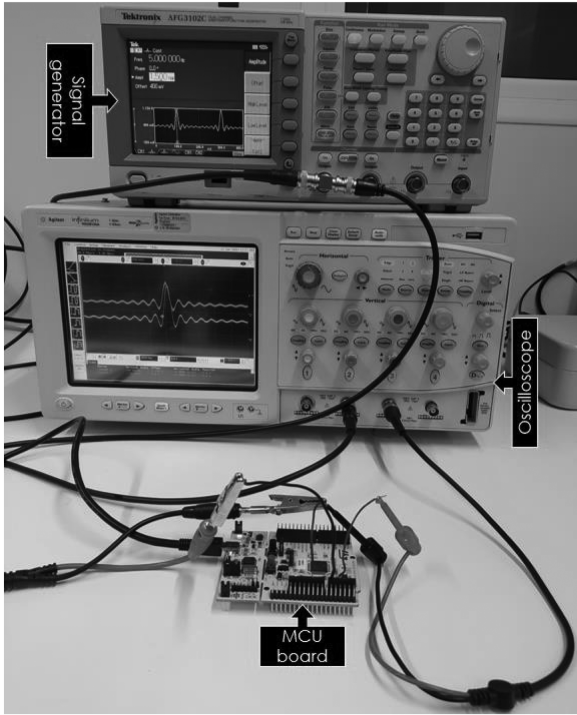
float zeta0 = 0.191; float zeta1 = -7.9; float zeta2 = 8.71;
float vin_1 = 0; float vin_0 = 0; float vout_1 = 0; float vout_0 = 0;
return float Process(float input)
{
//Update internally stored output at t-1
vout_1 = vout_0;
//Update internally stored input at t-1
vin_1 = vin_0;
//Update internally stored input at t
vin_0 = input;
//Compute output
vout_0 = zeta0*vout_0+ zeta1*vin_0+ zeta2*vin_1;
return vout_0;
}

```

Fig. 7. Numerical LP-NGD circuit code.



(a)



(b)

Fig. 8. (a) Illustrative diagram and (b) photograph of the LP-NGD MCU-based experimental setup.

TABLE I
TEST EQUIPMENT SPECIFICATIONS

| Description | Reference | Parameter | Value |
|------------------------------|---------------------------------|---------------|---------|
| Arbitrary function generator | Tektronix AFG3102C DUAL CHANNEL | Sampling rate | 1 GS/s |
| | | Bandwidth | 100 MHz |
| Digital oscilloscope | Agilent infiniium MSO8104A | V_{min} | 12.5 mV |
| | | Sampling rate | 4 GSa/s |
| | | Bandwidth | 1 GHz |
| | | Channels | 4 |

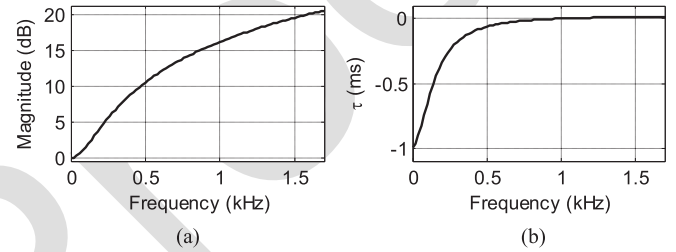


Fig. 9. LP-NGD frequency responses: (a) magnitude and (b) GD.

During the test, the oscilloscope input impedance is configured as $R_{in} = 1 \text{ } \Omega$. The employed test equipment specifications are addressed in Table I. Then, the tested signals are recorded in csv format and replotted in MATLAB environment. It is noteworthy that the MCU latency is about $21 \text{ } \mu\text{s}$.

C. Demonstration of Time < 0 Signal Prediction

This section discusses the demonstration results with three types of sensors. Prediction of arbitrary waveform signals in different time-scales is presented. The Gaussian pulse and sinc wave pulse signals were chosen for the LP-NGD time-domain validation because of the following reason.

- 1) They present a limited bandwidth, which can be assumed as the LP-NGD circuit cutoff frequency.
- 2) They enable to calculate the pulse duration in function of the LP-NGD circuit cutoff frequency.
- 3) To show the LP-NGD signature with the time-advance of leading- and tailing-edge between the input and output pulses.
- 4) To demonstrate the signal integrity by comparing the pulsewidth and amplitudes.
- 5) And to measure the magnitude effect by comparing the maximum peaks of input and output pulse signals.

1) LP-NGD Function Frequency Responses: Before the transient test, the LP-NGD circuit were synthesized under the desired specifications, static gain $N_0 = 0 \text{ dB}$, cutoff frequency $f_n = 1 \text{ kHz}$, and NGD value $\tau_n = -1 \text{ ms}$. Fig. 9 plots the magnitude and GD frequency responses from MATLAB computations of TF (5) in from dc to 1.7 kHz. These results confirm the LP-NGD behavior varying from -1 ms to 0 ms in the LF interval [0 Hz, 1 kHz] of the synthesized circuit. It is noteworthy that the gain at the cutoff frequency is approximately 17 dB. A limited bandwidth smoothed enough signal must be considered to realize the

268 Fig. 8(a), the input pulse analog voltage provided by the signal
 269 generator attacks the MCU and visualized simultaneously with
 270 the output analog voltage from pin PA5. The MCU is powered
 271 by USB port connected to the driver PC. Fig. 8(b) displays the
 272 photo of the performed experimental setup. As photographed by
 273 Fig. 8(b), the input and output analog signals are transmitted to
 274 the oscilloscope through a 1m-long cable.

TABLE II
SPECIFICATIONS OF THE INPUT GAUSSIAN SIGNALS, AND COMPARISON OF
SIMULATED AND CALCULATED LP-NGD TRANSIENT SPECIFICATIONS

| Parameter | V_{max} | a | f_a | t_0 |
|-------------|-------------------|-------------------|--------|----------|
| Value | 1 V | 10 dB | 200 Hz | 8.9 ms |
| Approach | Δt_{rise} | Δt_{fall} | a | ϖ |
| Calculation | -0.58 ms | -1.26 ms | 1.05 | 92.7% |
| Measurement | -0.57 ms | -0.97 ms | 1.11 | 93.5% |

time-domain effect of the LP-NGD function. For this reason, the preliminary frequency domain analysis is necessary before the LP-NGD in the time-domain. To complete validation of the numerical LP-NGD function, time-domain measurement results will be examined in the following paragraph.

2) Time < 0 Demonstration With Numerical LP-NGD Gaussian Response: The LP-NGD transient analysis must be performed with smoothed signal presenting spectrum belonging to the NGD frequency band. Accordingly, the Gaussian waveform pulse as input test signal is analytically expressed as

$$v_{in}(t) = V_{max} e^{-(t-t_0)^2/\tau_a^2} \quad (21)$$

with maximal peak $V_{max} = v_{in}(t_0)$, at instant time t_0 , and spectrum bandwidth depending to the time parameter [38]

$$\tau_a = \sqrt{a_{dB} \ln(10)/5}/(\pi f_a) \quad (22)$$

where a_{dB} is the Gaussian spectrum attenuation at frequency f_a . Knowing the maximal instant time t_0 , the LP-NGD circuit transient characterization can be performed by rise-time advance $\tau_r = t_r^{out} - t_r^{in}$, and fall-time advance $\tau_f = t_f^{out} - t_f^{in}$, with $v_{in}(t_r^{in} < t_0) = \max[v_{in}(t)]/2$ and $v_{out}(t_r^{out} < t_0) = \max[v_{out}(t)]/2$, combined to voltage gain between the input and output signals

$$a = \max[v_{out}(t)] / \max[v_{in}(t)]. \quad (23)$$

And also, the input and output relative cross-correlation can be written as

$$\varpi(v_{in}, v_{out}) = \frac{\sum_{k=1}^{k_{max}} [v_{in}(k) - \hat{v}_{in}] [v_{out}(k) - \hat{v}_{out}]}{\sqrt{\sum_{k=1}^{k_{max}} [v_{in}(k) - \hat{v}_{in}]^2} \sqrt{\sum_{k=1}^{k_{max}} [v_{out}(k) - \hat{v}_{out}]^2}} \quad (24)$$

where the input and output average values, $\hat{v}_{in} = \sum_{k=1}^{k_{max}} v_{in}(k)/k_{max}$ and $\hat{v}_{out} = \sum_{k=1}^{k_{max}} v_{out}(k)/k_{max}$.

The transient calculation was carried out with Gaussian signal with $t_{max} = 20$ ms and different parameters indicated by Table II. During the calculation, the time step was fixed to 0.1 ms and the IIR coefficients defined in (20) are $\{\zeta_0 = 0.191, \zeta_1 = -7.9, \zeta_2 = 8.71\}$. Fig. 10(a) displays the comparison between the MATLAB modeled v_{out_C} (black dashed curve), and measured, v_{out_M} (red dashed curve), output signals of Gaussian input (blue solid curve) defined by (21). The tested LP-NGD IIR is defined by coefficients $\{\zeta_0 = 0.553, \zeta_1 = -22.91, \zeta_2 = 23.36\}$. For the present case of Gaussian response, considerable output uncontested time-advances are obtained for both leading- and tailing-edges. Based on this good correlation between model

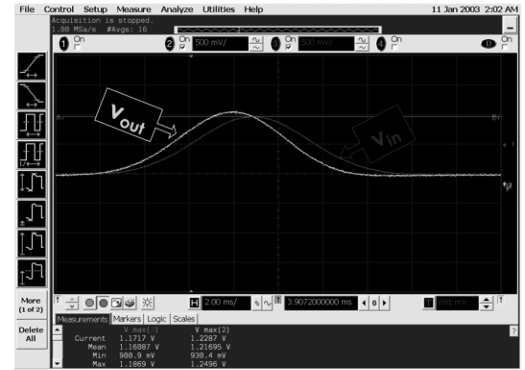
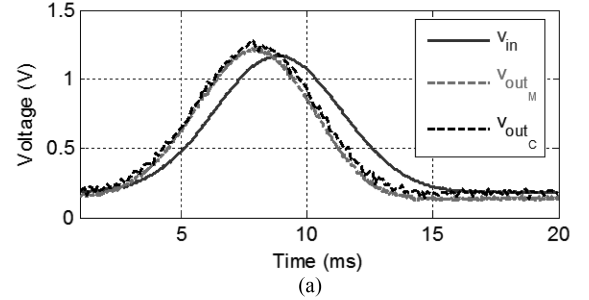


Fig. 10. (a) Calculated and measured LP-NGD MCU transient Gaussian pulse responses. (b) Corresponding oscilloscope screenshot of tested signals.

and measurement, the unfamiliar aspect of time advance is observed, which is a typical signature of LP-NGD function transient response. This sensational real-time result visualized by the screenshot Fig. 10(b) is the first time experimental and calculation validation of numerical LP-NGD circuit.

Moreover, Table II summarizes the LP-NGD transient characterization parameters. It is noteworthy that the numerical LP-NGD MCU input and output signal cross correlations are better than 92%.

The generality of the sensational time-advance was validated with two different arbitrary waveform and time-scale signals as explored in the following paragraphs.

3) Numerical LP-NGD Sinc Waveform Signal Response: Another transient test of the LP-NGD numerical circuit was performed with 10-ms pulse duration and 1-V peak-to-peak amplitude sinc waveform. The considered sinc signal presents a frequency spectrum belonging into the NGD frequency band. Fig. 11(a) displays the comparison between the calculated v_{out_C} and measured v_{out_M} . Once again, the output signal time-advance was observed, as seen in the screenshot of Fig. 11(b). During the calculation, the time step was fixed to 0.1 ms. Once again, based on this result showing about -1 ms time advance average of output sinc leading and trailing edges, the STM32 MCU is able to operate as a LP-NGD numerical circuit. In this case, based on formula (24), measured and calculated output signals have a relative cross-correlation of about 89.3% and 87.7%. In addition to the signal generator input signal test, computational investigation with more industrial context of sensed arbitrary waveform signals plotted in several hours and very long-time duration is examined in the following paragraph.

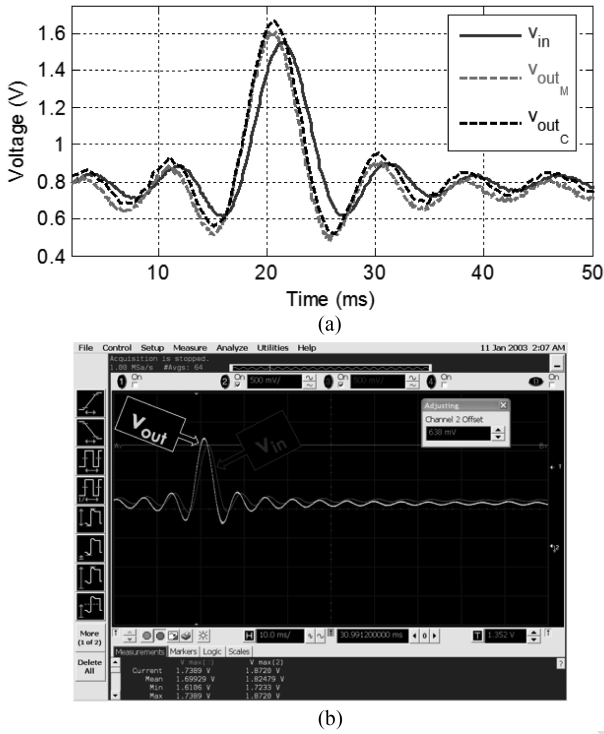


Fig. 11. (a) Calculated and measured LP-NGD MCU transient sinc waveform signal responses. (b) Corresponding oscilloscope screenshot of tested signals.

TABLE III
TEMPERATURE AND HUMIDITY WIRELESS SENSOR CHARACTERISTICS

| Measured parameter | Range | Accuracy | Type of sensor |
|--------------------|----------------|---------------------------------|--------------------|
| Temperature | -40°C to 125°C | +/- 0.4°C (max), at -10 to 85°C | Thermistor |
| Relative humidity | 0 to 100% | +/-3% (max), at 0 to 80% | Capacitive polymer |

372 **4) Hour Time-Scale Arbitrary Sensored Signal Prediction:**
 373 An illustrative industrial application case of LP-NGD
 374 function is described in this paragraph by using realm data
 375 recorded from temperature and humidity sensors. The realm data
 376 used in this paragraph were collected by sensors deployed on a
 377 student residence located in Douai city, in the north of France
 378 [39]. The adopted technology is wireless sensor network plat-
 379 forms based on a universal solution of the CLEODE company.
 380 Each smart-meter/device is set with a sampling time of $T_s = 2.4$
 381 min, and its characteristics are given in Table III. Thus, these
 382 configurations allow us to monitor the external environment
 383 of buildings. Fig. 12 illustrate the evolution of the outdoor
 384 climate during the experimentation (from Feb. 9, 2019 to Feb.
 385 21, 2019). On the top, we have the evolution of the outdoor
 386 temperature. That can take a value between 2 °C to 10 °C. In
 387 the bottom, we have the outdoor relative humidity. This last can
 388 take a value between 75% to 100%. In this case, the numerical
 389 LP-NGD function was synthesized under characteristics shown

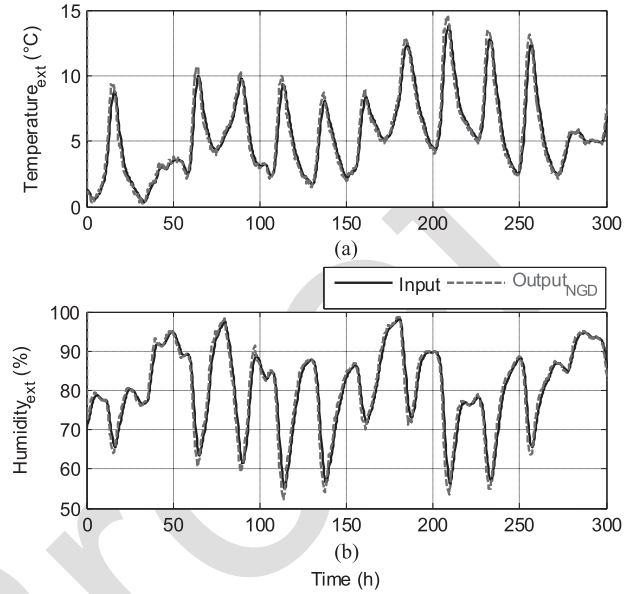


Fig. 12. LP-NGD responses of (a) temperature and (b) humidity sensors.

TABLE IV
NGD FUNCTION SPECIFICATIONS, AND TEMPERATURE AND HUMIDITY CROSS-CORRELATION

| Specifications | τ_n | f_n | ϖ |
|-------------------|----------|--------------|----------|
| Temperature | -1 h | 278 μ Hz | 81.8% |
| Relative humidity | | | 92.4% |

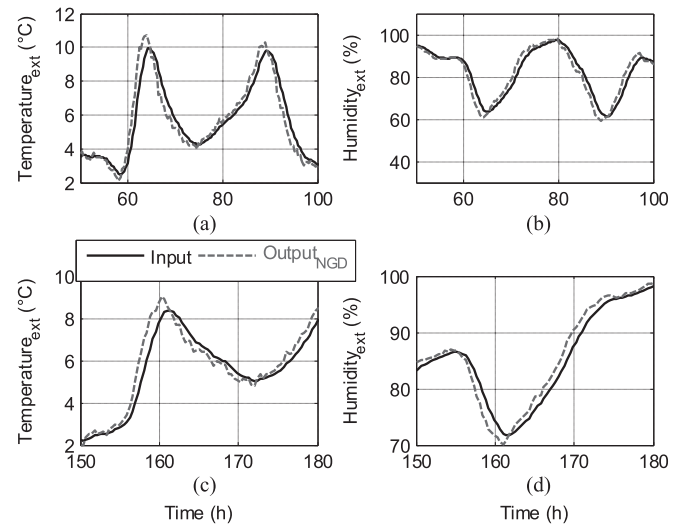


Fig. 13. Zoom in plots of LP-NGD responses of (a) [50 h, 100 h] and (b) [150 h, 180 h] time-interval temperature, and (c) [50 h, 100 h] and (d) [150 h, 180 h] time-interval humidity sensors.

in Table IV, $\tau_n = -3600$ s = -1 h and cutoff frequency, 390
 $f_n = 278$ μ Hz. 391

The feasibility study is based 300 h (h) or 12.5 days duration 392
 temperature and humidity measured sensed signals. The num- 393
 erical LP-NGD computed responses are presented in Fig. 12(a) 394

and (b). The cross correlation between the input–output temperatures and humidity’s are 81.8% and 92.4%, as tabulated in Table IV, respectively. As illustrated by the time-domain results zoomed in time-intervals [50 h, 100 h] [see Fig. 13(a) and (c)], and [150 h, 180 h] [see Fig. 13(b) and (d)], an exciting result showing prediction of signal waveform is observed with output advance compared to the input under medium time-advance of about 1 h.

IV. CONCLUSION

The first-time investigation on design and test of LP-NGD numerical circuit was developed. The LP-NGD function was originally designed and emulated on STM32 MCU board [37]. An innovative theory of LP-NGD IIR TF was established. The main specifications of the input signal susceptible to operate with the LP-NGD function were defined in function of the MCU specifications. The design method and implementation of the numerical LP-NGD function was described. Then, the canonical fundamental discrete function of LP-NGD numerical circuit was analytically introduced. The LP-NGD analysis and synthesis methodology was originally formulated in function of the NGD specifications.

To validate the numerical LP-NGD function, an original experimental setup with STM32 MCU board was considered as a POC. The numerical LP-NGD circuit was experimentally validated by millisecond short-duration and computationally validated by hour long-duration arbitrary waveform signal testing. Results showed a very good agreement between the analytical computations and experimentations were introduced and discussed. The numerical LP-NGD function industrial application was promisingly highlighted by arbitrary waveform sensed signals representing temperature and humidity 12.5-day duration data from embedded sensors.

Compared with the traditional LP-NGD analog circuit, the investigated numerical NGD circuit presents.

- 1) Benefits on i) the possibility to operate with long period signals having a duration of more than ten seconds (which cannot be treated with analog NGD circuits), ii) to interface the NGD circuit directly to digital signals, iii) to increase the order of LP-NGD circuit in order to widen the NGD bandwidth without increasing the physical size of the PCB prototype, and 4) to adjust negative delay programmatically according to the needs, making it versatile for a wide range of applications.
- 2) Disadvantages on i) the latency of the digital computations and ii) the delay introduced by ADC and DAC impacting the NGD response. However, especially for long NGD targeted by this digital implementation, conversion delays are usually negligible.

With this article, we envisage a revolution NGD technology for the future smart factories based on the sensed signal anticipation. To do this, the NGD MCU concept can be integrated in real-time simulation and deep learning interfaces [35], [36].

REFERENCES

- [1] A. Maiti, A. A. Kist, and A. D. Maxwell, “Real-time remote access laboratory with distributed and modular design,” *IEEE Trans. Ind. Electron.*, vol. 62, no. 6, pp. 3607–3618, Jun. 2015.
- [2] S. Liu, X. Wang, and P. X. Liu, “Impact of communication delays on secondary frequency control in an islanded microgrid,” *IEEE Trans. Ind. Electron.*, vol. 62, no. 4, pp. 2021–2031, Apr. 2015.
- [3] X. Lei, Y. Song, X. Yao, B. Dong, and M. Jin, “Effect of group delay on channel estimation performance in OFDM system,” *Appl. Math. Inf. Sci.*, vol. 6-3S, no. 3, pp. 1037–1045, 2012.
- [4] P.-Y. Chen, S. Yang, and J. A. McCann, “Distributed real-time anomaly detection in networked industrial sensing systems,” *IEEE Trans. Ind. Electron.*, vol. 62, no. 6, pp. 3832–3842, Jun. 2015.
- [5] N. Jalili and E. Esmailzadeh, “Optimum active vehicle suspensions with actuator time delay,” *Trans. ASME*, vol. 123, no. 1, pp. 54–61, Mar. 2001.
- [6] F. Wilches-Bernal *et al.*, “Effect of time delay asymmetries in power system damping control,” in *Proc. IEEE Power Energy Soc. Gen. Meeting*, Chicago, IL, USA, Jul. 16–20, 2017, pp. 1–5.
- [7] A. Pal, R. Kumar, and S. Das, “Stability and dynamic performance improvement of adaptive full-order observers in sensorless induction motor drives,” *Energy Procedia*, vol. 90, pp. 540–551, Dec. 2016.
- [8] A. B. Kahng and S. Muddu, “An analytical delay model of RLC interconnects,” *IEEE Trans. Comput.-Aided Des. Integrated Circuits Syst.*, vol. 16, no. 12, pp. 1507–1514, Dec. 1997.
- [9] R. Venkatesan, J. A. Davis, and J. D. Meindl, “Compact distributed RLC interconnect models - part IV: Unified models for time delay, crosstalk, and repeater insertion,” *IEEE Trans. Electron Devices*, vol. 50, no. 4, pp. 1094–1102, Apr. 2003.
- [10] S. Roy and A. Dounavis, “Efficient delay and crosstalk modeling of RLC interconnects using delay algebraic equations,” *IEEE Trans. Very Large Scale Integration*, vol. 19, no. 2, pp. 342–346, Feb. 2011.
- [11] B. Ravelo, “Delay modelling of high-speed distributed interconnect for the signal integrity prediction,” *Eur. Phys. J. Appl. Phys.*, vol. 57, Feb. 2012, Art. no. 31002.
- [12] Z. S. Veličković and V. D. Pavlović, “Complex analytic signals applied on time delay estimation,” *Phys., Chem. Technol.*, vol. 6, no. 1, pp. 11–28, 2008.
- [13] S.-S. Myoung, B.-S. Kwon, Y.-H. Kim, and J.-G. Yook, “Effect of group delay in RF BPF on impulse radio systems,” *IEICE Trans. Commun.*, vol. 90, no. 12, pp. 3514–3522, Dec. 2007.
- [14] G. Groenewold, “Noise and group delay in active filters,” *IEEE Trans. CAS I, Regular Papers*, vol. 54, no. 7, pp. 1471–1480, Jul. 2007.
- [15] L. Clifton, D. A. Clifton, M. A. F. Pimentel, P. J. Watkinson, and L. Tarassenko, “Predictive monitoring of mobile patients by combining clinical observations with data from wearable sensors,” *IEEE J. Biomed. Health Inform.*, vol. 18, no. 3, pp. 722–730, May 2014.
- [16] L. M. Nilsson, “Respiration signals from photoplethysmography,” *Anesthesia Analgesia*, vol. 117, no. 4, pp. 859–865, Oct. 2013.
- [17] J. L. Moraes, M. X. Rocha, G. G. Vasconcelos, J. E. Vasconcelos Filho, V. H. C. de Albuquerque, and A. R. Alexandria, “Advances in photoplethysmography signal analysis for biomedical applications,” *Sensors*, vol. 18, no. 6, pp. 1–26, Jun. 2018.
- [18] J. W. Chong *et al.*, “Photoplethysmograph signal reconstruction based on a novel hybrid motion artifact detection–reduction approach. Part I: Motion and noise artifact detection,” *Ann. Biomed. Eng.*, vol. 42, no. 11, pp. 2238–2250, Nov. 2014.
- [19] A. S. Junior, A. Spirandeli, R. Moraes, and V. Zazoso, “Respiratory waveform estimation from multiple accelerometers: An optimal sensor number and placement analysis,” *IEEE J. Biomed. Health Inform.*, vol. 23, no. 4, pp. 1507–1515, Jul. 2019.
- [20] C. Hymel, R. A. Stubbers, and M. E. Brandt, “Temporally advanced signal detection: A review of the technology and potential applications,” *IEEE Circuits Syst. Mag.*, vol. 11, no. 3, pp. 10–25, Jul.–Sep. 2011.
- [21] H. U. Voss, “Signal prediction by anticipatory relaxation dynamics,” *Phys. Rev. E*, vol. 93, no. 3, 2016, Art. no. 030201R.
- [22] H. U. Voss and N. Stepp, “A negative group delay model for feedback-delayed manual tracking performance,” *J. Comput. Neurosci.*, vol. 41, no. 3, pp. 295–304, Dec. 2016.
- [23] K.-P. Ahn, R. Ishikawa, and K. Honjo, “Group delay equalized UWB ingap/gaas HBT MMIC amplifier using negative group delay circuits,” *IEEE Trans. Microw. Theory Techn.*, vol. 57, no. 9, pp. 2139–2147, Sep. 2009.

448
449
450
451
452
453
454
455
456
457
458
459
460
461
462
463
464
465
466
467
468
469
470
471
472
473
474
475
476
477
478
479
480
481
482
483
484
485
486
487
488
489
490
491
492
493
494
495
496
497
498
499
500
501
502
503
504
505
506
507
508
509
510
511
512
513
514
515
516
517
518
519
520

- [24] D. Solli, R. Y. Chiao, and J. M. Hickmann, "Superluminal effects and negative group delays in electronics, and their applications," *Phys. Rev. E*, vol. 66, 2002, Art. no. 056601.
- [25] F. Wan *et al.*, "Design of multi-scale negative group delay circuit for sensors signal time-delay cancellation," *IEEE Sensors J.*, vol. 19, no. 19, pp. 8951–8962, Oct. 2019.
- [26] M. W. Mitchell and R. Y. Chiao, "Causality and negative Group-delays in a simple bandpass amplifier," *Amer. J. Phys.*, vol. 66, no. 1, pp. 14–19, Nov. 1998.
- [27] M. W. Mitchell and R. Y. Chiao, "Negative Group-delay and 'Fronts' in a causal systems: An experiment with very low frequency bandpass amplifiers," *Phys. Lett. A*, vol. 230, no. 3/4, pp. 133–138, Jun. 1997.
- [28] T. Nakanishi, K. Sugiyama, and M. Kitano, "Demonstration of negative Group-delays in a simple electronic circuit," *Amer. J. Phys.*, vol. 70, no. 11, pp. 1117–1121, 2002.
- [29] M. Kitano, T. Nakanishi, and K. Sugiyama, "Negative Group-delay and superluminal propagation: An electronic circuit approach," *IEEE J. Sel. Topics Quantum Electron.*, vol. 9, no. 1, pp. 43–51, Feb. 2003.
- [30] B. Ravelo, "Similitude between the NGD function and filter gain behaviours," *Int. J. Circuit Theor. Appl.*, vol. 42, no. 10, pp. 1016–1032, Oct. 2014.
- [31] B. Ravelo, "First-order low-pass negative group delay passive topology," *Electron. Lett.*, vol. 52, no. 2, pp. 124–126, Jan. 2016.
- [32] F. Wan *et al.*, "Negative group delay theory of a four-port RC-Network feedback operational amplifier," *IEEE Access*, vol. 7, no. 1, pp. 75708–75720, Dec. 2019.
- [33] C. Kwan and R. Xu, "A note on simultaneous isolation of sensor and actuator faults," *IEEE Trans. Control Syst. Technol.*, vol. 12, no. 1, pp. 183–192, Jan. 2004.
- [34] N. Zhou, L. Luo, G. Sheng, and X. Jiang, "High accuracy insulation fault diagnosis method of power equipment based on power maximum likelihood estimation," *IEEE Trans. Power Del.*, vol. 34, no. 4, pp. 1291–1299, Aug. 2019.
- [35] Y. Chen and V. Dinavahi, "Hardware emulation building blocks for real-time simulation of large-scale power grids," *IEEE Trans. Ind. Inform.*, vol. 10, no. 1, pp. 373–381, Feb. 2014.
- [36] L. V. D. Maaten and G. Hinton, "Visualizing data using t-SNE," *J. Mach. Learn. Res.*, vol. 9, pp. 2579–2605, Nov. 2008.
- [37] ST, STM32L476xx, Datasheet-Production Data, pp. 1–270, Jun. 2019.
- [38] R. Vauche *et al.*, "High efficiency UWB pulse generator for ultra-low-power applications," *Int. J. Microw. Wireless Technol.*, vol. 8, no. 3, pp. 495–503, May 2016.
- [39] L. Rajaoarisoa, B. Ravelo, W. Rahajandraibe, and L. Etienne, "Weather prediction to improve energy efficiency and climate control of the buildings," in *Proc. IBPSA France*, Nov. 12/13, 2020, pp. 1–7.



Blaise Ravelo (Member, IEEE) is currently a University Full Professor with the Nanjing University of Information Science and Technology, Nanjing, China. His research interests include on multiphysics and electronics engineering.

Prof. Ravelo is a Pioneer of the Negative Group Delay (NGD) concept about $t < 0$ signal travelling physical space. He was research director of 11 Ph.D. students (eight defended), postdocs, research engineers, and Master internships. With US, Chinese, Indian, European,

and African partners, he is actively involved and contributes on several international research projects (ANR, FUI, FP7, INTERREG, H2020, Euripides², Eurostars...). He is Member of IET Electronics Letters Editorial Board as Circuit and System Subject Editor. He is ranked in Top 2% world's scientists based on years 2019 by Stanford University, US. He has Google scholar h-index (2021) = 23 and i10-index(2021) = 68. He is member of research groups: IEEE, URSI, GDR Ondes, Radio Society and (co-) authors of more than 360 scientific research papers in new technologies published in International Conference and Journals. He is Lecturer on Circuit and System Theory, STEM (science, technology, engineering, and maths) and applied physics. He is regularly invited to review papers submitted for publication to international journals (IEEE TRANSACTIONS ON MICROWAVE THEORY AND TECHNIQUES, IEEE TRANSACTIONS ON CIRCUITS AND SYSTEMS, IEEE TRANSACTIONS ON ELECTROMAGNETIC COMPATIBILITY, IEEE TRANSACTIONS ON INDUSTRIAL ELECTRONICS, IEEE ACCESS, *IET Circuits, Devices, and Systems*, and *IET Microwaves, Antennas and Propagation*) and books (Wiley, Intech Science).



Mathieu Guerin (Member, IEEE) received the Engineering degree in microelectronics and telecommunications from Polytech Marseille, Marseille, France, and the Research Master degree in integrated circuits design from the University of Aix-Marseille, Marseille, France, both in 2010, and the doctorate degree from the University of Aix-Marseille, in 2010.

He was a Technical Leader of the Analog and Radio-Frequency Design Team of IDEMIA-StarChip for five years and designed chips embedded in SIM cards and contactless bank cards with biometric recognition. He joined Aix-Marseille University as an Assistant Professor in 2020 and joined the CCSI Team of the IM2NP Laboratory. He is working on methods of modeling and characterizing circuits in analog electronics. His research interest includes the design and synthesis of circuits in digital electronics.



Wencleslas Rahajandraibe (Member, IEEE) received the B.Sc. degree in electrical engineering from Nice Sophia-Antipolis University, Nice, France, in 1996, the M.Sc. degree (with distinction) in electrical engineering from the Science Department, University of Montpellier, Montpellier, France, in 1998, and the Ph.D. degree in microelectronics from the University of Montpellier.

He is currently a Full Professor with the University of Aix-Marseille, Marseille, France. Since 1998, he has been with the Microelectronics Department of Informatics, Robotics and Microelectronics, Laboratory of Montpellier (LIRMM). Since 2003, he has been with the Microelectronic Department of Materials, Microelectronics and Nanoscience, Laboratory of Provence (IM2NP), Marseille, France, where he was an Associate Professor. Since 2014, he has been a Professor with Aix Marseille University where he heads the Integrated Circuit Design group of the IM2NP Laboratory. He is regularly involved to participate and to lead national and international research projects (ANR, H2020, FP7 KIC-InnoEnergy...). He directed and cosupervised 18 Ph.D. and 15 Master students. He has authored or coauthored 11 patents and more than 150 papers published in refereed journals and conferences. His research interests include AMS and RF circuit design from transistor to architectural level. His current research interests include ultralow power circuit design for smart sensor interface and embedded electronic in bioelectronic and e-health applications, wireless systems, design technique, and architecture for multistandard transceiver.

Prof. Rahajandraibe is an Expert for the ANR, the French Agency for Research. He has served on program committees of IEEE INTERNATIONAL NEW CIRCUITS AND SYSTEMS CONFERENCE and IEEE INTERNATIONAL CONFERENCE ON ELECTRONICS, CIRCUITS, AND SYSTEMS. He has been and is a Reviewer of contributions submitted to several IEEE conferences and journals such as IEEE INTERNATIONAL SYMPOSIUM ON CIRCUITS AND SYSTEMS, IEEE INTERNATIONAL NEW CIRCUITS AND SYSTEMS CONFERENCE, IEEE INTERNATIONAL MIDWEST SYMPOSIUM ON CIRCUITS AND SYSTEMS, ESSCIRC, ESSDERC, RFIC, IEEE TRANSACTIONS ON CIRCUITS AND SYSTEMS I AND II, *IET Electronics Letters*.



Valentin Gies (Member, IEEE) received the Graduate degree in applied physics from Ecole Normale Supérieure, Paris, France, in 2001, and the Ph.D. degree in electronics from Ecole Nationale Supérieure de Techniques Avancées, Paris XI Orsay University, Orsay, France, in 2005.

His Ph.D. was focused on both circuits and algorithms for artificial Retinas. He is Lecturer and Researcher with Toulon University since 2007, and an Associate Professor in Robotics, Embedded Electronics and IoT at SeaTech, ISEN Toulon, and ENSTA ParisTech. He was with the IM2NP CNRS Laboratory in 2017, in the Circuits Design Team. His current research interests include embedded algorithms and circuits for ultralow power systems.

Prof. Gies is Scientific Advisor of several start-ups in IoT and Head of Scientific Microsystems for Internet of Things, Toulon University.

Q5
Q6

Q7

596
597
598
599
600
601
602
603
604
605
606
607
608
609
610
611
612
613614
615
616
617
618
619
620
621
622
623
624
625
626
627
628
629
630
631
632
633
634
635
636
637
638
639
640
641
642
643
644
645
646
647
648
649
650
651652
653
654
655
656
657
658
659
660
661
662
663
664
665
666
667
668
669

Q3

Q4

670
671
672
673
674
675
676
677
678
679
680
681
682
683
684
685
686
687
688
689
690



Lala Rajoarisoa (Member, IEEE) received the M.Sc. and Ph.D. degree in automatic and computer sciences from the University of Aix-Marseille, Marseille, France, in 2005 and 2009, respectively.

He is currently an Assistant Professor with the Institut Mines-Télécom Lille Douai. Develop predictive models and controllers to assess system behavior and optimize its performance. This development includes the analysis of intrinsic properties such as stability, observability, identifiability, and controllability. He is involved in research activities dedicated to the optimization of energy efficiency of building systems and the control and management of hydraulic systems with more than 80 papers published in refereed journals and conferences. He regularly participates and contributes on several international projects (ANR, FUI, and INTERREG) and was the supervisor of more than of 15 Ph.D. students, postdocs, research engineers, and Master internships. His research interests include the development of data-driven tools and methods for the observation and control of large-scale distributed systems.



Sébastien Lalléchère (Member, IEEE) was born in Nevers, France, in 1979. He received the M.Sc. and Ph.D. degrees in computational modeling and electronics/electromagnetism from Polytech Clermont and Université Blaise Pascal, Clermont-Ferrand, France, in 2002 and 2006, respectively.

He was Research Engineer with LASMEA, Clermont-Ferrand, France, in 2007 focusing on intensive computational methods for electromagnetics. He is currently an Associate Professor with the Institut Pascal and Université Clermont Auvergne, Clermont-Ferrand, France. His research interests include electromagnetic compatibility including antennas and propagation, complex and reverberating electromagnetic environments, electromagnetic coupling, computational electromagnetics, stochastic modeling, and sensitivity analysis in electrical engineering.

691
692
693
694
695
696
697
698
699
700
701
702
703
704
705
706
707
708

IEEE PROCEEDINGS